FINITE ELEMENT ANALYSIS OF COLD FLAT ROLLING OF STRAIN HARDENING MATERIALS

By

REGALLA SRINIVASA PRAKASH

DEPARTMENT OF MECHANICAL ENGINEERING

INDIAN INSTITUTE OF TECHNOLOGY KANPUR

APRIL, 1992

FINITE ELEMENT ANALYSIS OF COLD FLAT ROLLING OF STRAIN HARDENING MATERIALS

A Thesis Submitted

In Partial Fulfilment of The Requirements

for the Degree of

MASTER OF TECHNOLOGY

by

REGALLA SRINIVASA PRAKASH

to the

DEPARTMENT OF MECHANICAL ENGINEERING

INDIAN INSTITUTE OF TECHNOLOGY KANPUR

APRIL , 1992

ME-1992-M-PRA-FIN

CERTIFICATE

It is certified that the work contained in the thesis entitled "FINITE ELEMENT ANALYSIS OF COLD FLAT ROLLING OF STRAIN HARDENING MATERIALS", by Regalla Srinivasa Prakash , has been carried out under our supervision and that this work has not been submitted elsewhere for a degree.

Dr. G.K.Lal
Professor
Mechanical Engineering
I.I.T. Kanpur.

Dr. P.M.Dixit
Assistant Professor
Mechanical Engineering
I.I.T. Kanpur.

April, 1992 .

ABSTRACT

The process of cold flat plane-strain rolling of rigid-plastic strain hardening materials is analyzed by Galerkin finite element technique coupled with the direct penalty method at steady state. Analysis is carried out both without and with strain hardening and the analytical results for normal pressure distribution, roll force and roll torque with strain hardening are compared with the experimental results. A detailed parametric study is carried out to show the effect of the process variables viz. reduction ratio, R/h_1 and the coefficient of friction on the important rolling design parameters of normal pressure distribution, roll separating force and roll torque. The percentage under estimation of these rolling parameters with the assumption of perfectly plastic material is highlighted. A study of contours of normal strain_rate, equivalent strain_rate, deviatoric stress and equivalent strain for four selected sets of process variables is presented. It is concluded that the present model is capable of estimating the important rolling parameters for a range of process variables and easily accommodates experimentally measured variable coefficient of friction for estimating more accurate results.

ACKNOWLEDGEMENTS

I acknowledge with sincerity and deep sense of gratitude the expert guidance and continuous encouragement provided by Dr. G.K.Lal and Dr. P.M.Dixit throughout the course of this thesis. I also thank them for their contributions made by the way of advice and criticism at various stages of this work.

I thank the entire staff of the computer center, IIT Kanpur, for enabling me to carry out the computations without any major interruption,albeit some occasional shutdowns.

I wish to thank all my friends, neighbor and acquaintances in the campus for making my stay at IIT Kanpur memorable.

Regalla Srinivasa Prakash

April, 1992

I.I.T. Kanpur.

TO

MY BELOVED PARENTS

CONTENTS

LIST OF TABLES

page no.

LIST OF FIGURES

LIST OF NOTATIONS

Symbol	Description
A	Area of the Domain
A^e	Area of an Element
B	Matrix of Differential Coefficients of Shape Functions
f	Average Coefficient of Friction
f_b	Boundary Elemental Matrix
F	Global Load Matrix
h_1	Initial Thickness of the Work Piece
h_2	Final Thickness of the Work Piece
H	Matrix Containing Defferential Coefficients of Shape Functions,(A Part of the Matrix B,used for strains)
$\|J\|$	Determinant of the Jacobian Matrix
k_s	Relative Sign of Boundary Tractions
k^e	Elemental Area Matrix
k_1^e	Part of the Elemental Area Matrix Resulting from Momentum Equation
k_2^e	Part of the Elemental Area Matrix Resulting from

	Penalization
K	Global Stiffness Matrix
k_g^e	Elemental Coefficient Matrix for Strains
K_g	Global Coefficient Matrix for Strains
l_i	Length of the Inlet Zone
l_o	Length of the Exit Zone
m	Multiplication Matrix
n	Multiplication Factor for the Calculation of inlet and exit zone lengths
nbelem	Number of Boundary Elements
nelem	Number of Domain Elements
n_x	Unit Normal Component in X-Direction
n_y	Unit Normal Component in Y-Direction
$\hat{n}$	Unit Normal Vector
N^1	One-Dimensional matrix of Biquadratic Shape Functions
N_v	Matrix of Biquadratic Shape Functions for the Approximation of Velocities
p	Hydrostatic Pressure
r^e	Elemental Right Hand Side Vector for Strains
R	Global Right Hand Side
R	Roll Radius
$\underline{\underline{S}}$	Deviatoric Stress Tensor

S_{ij}	Deviatoric Stress Components
$\bar{S}$	Deviatoric Stress Invarient
t	Matrix of Boundary Elemental Nodal Tractions
t_n	Normal Traction on the Work Piece-Roll Interface
t_s	Tangential Traction on the Work Piece-Roll Interface
t_x	Traction on the Work Piece-Roll Interface in the X-Direction
t_y	Traction on the Work Piece-Roll Interface in the Y-Direction
u	Velocity Component in X-Direction
u_n	Resultant Velocity Normal to the Interface
U_1	Known Velocity in X-Direction at the Inlet
U_2	Known Velocity in X-Direction at the Exit
v	Velocity Component in Y-Direction
V_1	Known Velocity in Y-Direction at the Inlet
V_2	Known Velocity in Y-Direction at the Exit
$\underline{V}$	Velocity Vector
V	Global Matrix of Nodal Velocities
V^e	Elemental Matrix of Nodal Velocities
W	Global Matrix of Nodal Weight Functions
w_s^e	Matrix of ElementalNodal Weight Functions for Strains

W_s	Global Matrix of Nodal Weight Functions for Strains
x	X-Coordinate
y	Y-Coordinate
α	Angle Made By the Normal to the Interface with Y-Axis at any point on the Interface
α_k	Angle at a Global Node on the Interface, k
α_n	Neutral Angle
∂	Partial Derivative Operator
∇	The Vector Differential Operator , Del
$\underline{\underline{\dot{\varepsilon}}}$	Strain Rate Tensor
$\dot{\varepsilon}_{ij}$	Strain Rate Components
$\dot{\varepsilon}'$	Deviatoric Part of the Strain Rate
$\bar{\dot{\varepsilon}}$	Equivalent Strain Rate
$\bar{\varepsilon}$	Equivalent Strain
Γ	The Boundary of the Domain
Γ^e	Elemental Boundary
λ	The Penalty Factor
$\bar{\lambda}$	Constant Used to Evaluate the Penalty Factor
ρ	Density
$\underline{\underline{\sigma}}$	The Stress Tensor
σ_{ij}	The Stress Components

σ_o	Initial Yield Stress of the Metal
σ_y	Variable Yield Stress of the Metal
ξ ,η	Natural Coordinates for Domain Elements
2μ	Proportionality Constant
μ_o	Constant Used for the Non-Dimensionalization of μ
ζ	Natural Coordinates for Boundary Elements

Subscripts

b	Boundary
v	Corresponding to the Velocities
s	Corresponding to the Strains or Tangential
o	Initial Value
n	Normal Component
1	Inlet
2	Exit
x	In the Direction of X-Axis
y	In the Direction of Y-Axis

Superscripts

be	Boundary Element
e	Domain Element
~	Non-dimensionalized Quantity

CHAPTER 1

INTRODUCTION

1.1. General Introduction

Rolling is one of the most important industrial metalworking processes because of its extensive use in the production of a large variety of industrial steel products. Moreover, as is evident from the extent of published literature since the beginning of this century, rolling is apparently one of the most investigated of all the known metal forming processes.

1.2. Mechanics of Rolling Process

In reality as the material approaches the rolls it first undergoes elastic deformation till it reaches the yield point and a large plastic deformation zone follows. As the material exits the deformation zone there will be an elastic spring back. However, the magnitude of the elastic strains is negligibly small compared to the large amounts of plastic deformation that the material undergoes during the rolling process. Typical orders of elastic and plastic strains usually found are 10^{-4} and 0.25 respectively. Therefore ignoring the elastic strains the material may be assumed to be rigid till it comes first in contact with the rolls and after it leaves the contact of the rolls . Further during the deformation process in the deformation zone the strains are totally plastic.

Many experimental and theoretical investigations have shown that the velocities,strains and stresses are not uniformly

distributed across the sections.The velocity across the sections of the work in the unstrained zone remains uniform while in the deformation zone the outer layers of the metal towards the rolls move faster than the inner layers. Near the entry the outer layers have a less velocity than the roll periphery. But the velocity of the outer layers (represented by V_s) of the work piece increases as it moves towards the exit and eventually it becomes more than the roll peripheral velocity(represented by V_r) as it reaches the exit. Although the transition occurs over a zone, because of the lack of exact data many researchers considered this as a point. The zone in which V_r is less than V_s is called forward slip region and in this region the friction force tends to retard the motion of the work piece. The point at which V_s is equal to V_r is called the neutral point.

Analytical expressions for the determination of the neutral point have been developed by some researchers. Notable among them is the Avitzur's formula [1]:

$$\alpha_n = \frac{1}{3}\sqrt{\frac{h_2}{R}}\left[\tan^{-1}\sqrt{\left(\frac{h_1}{h}-1\right)} - \frac{1}{m}\sqrt{\frac{h_2}{R}}\left\{\ln\left(\frac{h_1}{h}\right) + \frac{1}{4}\sqrt{\frac{h_2}{R}}\sqrt{\left(\frac{h_2}{h}-1\right)} + \frac{\sigma_{xb}-\sigma_{xf}}{(2/\sqrt{3})\sigma_o}\right\}\right]$$

The strain rates developed in the rolling process where the roll velocities are not very high are appreciably small. The entire work done by the tool in the plastic deformation of the workpiece is converted into heat leading to an increase in the

temperature of the workpiece. Strain-rates, temperatures and the strains that the material undergoes can affect its yield strength. However, the effect of the former two viz. strain-rate and temperature effects can be ignored in a cold rolling process since they are not substantially high whereas the strain hardening effect is substantial to be considered.

Unlike most of the other metal forming processes where the tool remains stationary, in the flat rolling process the rolls will also be in movement thus the mathematical modelling of the process is difficult. The friction coefficient constantly changes from point to point along the arc of contact becoming zero at the neutral point. Many analytical expressions have been proposed in the literature to model the friction behaviour at the interface in the rolling process but none has predicted its variation correctly.

For a successful design of rolling equipment and the process proper the important parameters to be considered are the normal pressure distribution along the interface, roll separating force and the roll torque. Analytical estimation of these parameters entails the analysis of the strainrates, strains in the workpiece during the deformation process.

1.3. Previous Work

Many researchers carried out a variety of analytical and experimental investigations on the complex problem of rolling process.

The pioneering work on the theory of rolling was done by von Karman [2] in 1925, and then by Orowon [3] in 1943. As per the

review given in [5], von Karman introduced for the first time the slab method of analysis where the assumption of planes remain was made, while the later work came out to be one of the most comprehensive of all analytical studies where Orowon accounted for all the various phenomena of rolling process and developed a differential equation. Orowon could not give an analytical solution to it but he presented a graphical solution. Considering the complexity of Orowon's equations,the later researchers, especially Bland & Ford [4] introduced some simplifying assumptions and developed analytical expressions. Alexandar[5] presented a comprehensive solution to Von Karman's original differential equation without taking into consideration the effects of inhomogeneity of deformation. Lahoti et al [6] combined the best of the theories then existing and solved for temperatures,roll separating force and roll torque with the aid of a computer-aided simulation and compared his results with the experiments in the literature. Numerous slip-line field and upper-bound solutions have also been proposed for the plain-strain rolling case. A few popular ones are the Alexander's [7] slip-line field solution for hot rolling, the slip-line field solution of Firbank etal [8]for cold rolling and the only known upper bound solution of Jhonson etal [9]. The slip-line and upper bound techniques can give good solutions only to a limited number of cases and the material is invariably assumed to be perfectly plastic. The solution is also not unique in these cases.

The advent of the application of the powerful technique of finite element method to metal forming processes is of recent

past and it indeed paved a way to a great multitude of analytical solutions which till date have taken different turns towards the advancement in unraveling the problems involved in the rolling process, especially the neutral point phenomenon. The initial uses of FEM in metal forming problems were made by Ziekiewicz etal [10] and Dawson[11] who treated the rolling problem in terms of viscoplasticity where the metal is considered to flow as an incompressible non-Newtonian fluid with prescribed boundary velocities. Dawson also included the thermal analysis.G.J.Li.et al[12] have analyzed the problem of cold flat rolling by rigid-plastic finite element analysis by considering the friction relation developed by Chen and Kobayashi[13] . At the same time Mori etal [14] analyzed in the same direction but incorporated slight compressibility of the work material. Yhu et al [15] accounted for the variable coefficient of friction by using the experimental data in the literature and obtained a better correlation with the experimental results. Richelson [16] studied the effect of various friction models on the distribution of the normal and tangential tractions in cold plane-strain rolling using rigid-plastic FEM. However, the final important parameters of roll force and roll torque were not estimated in this work rendering it to be incomplete. An interesting case of asymmetric cold rolling was dealt with by Pietrzyk [17] where the problem of plane-strain rolling was analyzed with different angular velocities and different diameters of the rolls considered. The friction coefficient was used differently for the two rolls in the pair.Mori etal [18] tried to incorporate

the elastic deformation of the rolls by boundary element method while the strip was analyzed by rigid-plastic finite element method. It was illustrated that the normal pressure is lower with deformed rolls, than that with rigid rolls ,in contrast to what was believed by many researchers. Some 3-D analyses have been conducted by researchers notable among them are [19 - 24] .

A good number of experimental investigations have also been conducted in rolling. Al-Salehi et al [25] has presented a comprehensive set of experimental results by measuring the roll pressure distribution in the roll gap during cold metal rolling under plane-strain conditions for aluminium,copper and mild steel. The difference in pressure distribution with different R/h1 values was highlighted. It was shown that neutral point occurs in all cases of rolling very close to the exit. Roll force and roll torque values were measured and presented for aluminium and copper at various reduction ratios. Shida etal [26] have measured the roll force and roll torque in case of cold rolling of mild steel.

1.4. Objectives of the present thesis

From the above study of the finite element literature it is clear that while the initial works ignored the strain-hardening effect, the later investigations except for [15], considered a frictional relation in which the so called friction factor 'm' is used which does not seem to have any rational basis. Also few works have estimated the error which results from the assumption of perfectly plastic material. Some researchers did not determine the practically useful quantities like the roll force and roll torque while many others did not compare their results with any

experimental work.

In the present work the important design parameters of the rolling process viz. roll force, roll torque and normal pressure, shear stress distributions are estimated for various cases involving three metals under the plane-strain assumption and by considering the effect of strain hardening. For treating friction at the work piece-roll interface and to model the neutral point phenomenon, the traditional Coulomb's friction relation is used in which the average coefficient friction is taken from the same experimental works in the literature from which the analyzed cases are considered. The analytical results for roll force, roll torque and normal pressure distribution are compared with the experimental results. A detailed parametric study is carried out and the percentage error that is likely to accumulate with the ignorance of strain hardening effect is highlighted.

Determination of the above mentioned design parameters of the rolling process needs the knowledge of stress and strain distributions in the work piece. These are estimated by treating the rolling problem as a plane-strain steady state problem using Eulerian formulation with strain rate as the measure of deformation. The material is assumed to be rigid-plastic strain hardening. Temperature and strain-rate effects are ignored as these are usually small. For simplicity, the rolls are considered to be rigid. The domain includes sufficient portions of the inlet and exit zones to take the advantage of uniform conditions prevailing there. Galerkin weighed residual technique coupled with the direct penalty method is used for weak formulation. The domain

is discretized into small elements and biquadratic approximation for velocity components is used to convert the continuity and momentum equations into a set of nonlinear algebraic equations. These equations are solved by iteration. First a converged solution is obtained without the strain hardening effect. This solution is then used as the initial approximation to solve the system of equations for strain hardening problem. The knowledge of the equivalent strain required for updating the material properties at each iteration is obtained by integrating the equivalent strain rate. The converged solution for nodal velocities is used to estimate secondary quantities viz. strain rates,stresses,roll separating force, roll torque and normal pressure and the shear stress distributions.

Our modelling is such that the roll velocity is not required in our non-dimensional formulation.

1.5. Scope of the Present Work

In this analysis, the material is assumed to be rigid plastic strain hardening which yields according to the von Mises criterion. Although this assumption is valid in the deformation zone the elastic effects are significant at the entry and exit and therefore, should be included in the analysis. However, for simplicity, these effects are ignored in present analysis. The rolls are assumed to be rigid. Roll flattening has a propensity to decrease the roll forces since the effective reduction with elastically deformed rolls is lesser [18].

The effect of temperature and strain rate effects on the yield strength of the material are ignored in this work because of

the two reasons, besides the fact that their inclusion renders the analysis to be too complex. The first reason is that it is strongly expected that whatever the direct effect of strain-rate on the yield strength is present it is marginalized by the temperature softening. Secondly the roll speeds are not so high as to increase the strain rates to magnitudes. It is observable that no previous work has considered both strain and strain rate effects simultaneously.

The most important of all assumptions is that of average coefficient of friction. But in practice this is not the case where the coefficient of friction continuously varies along the interface, becoming zero at the neutral point.

The roll velocity can enter the problem only through the dependence of the yield stress on the strain rate or through the roll velocity dependent friction relation. But since we are not incorporating any of these two effects, there is no dependence of various parameters on the roll velocity in this formulation.

The present analysis investigates into the applicability of the traditional Coloumb's friction relation for the treatment of the friction at the workpiece-roll interface in the problem of cold flat plane-strain rolling of plates where the width of the plate is considerably large compared to its thickness, at steady state. In this relation the frictional stress is a constant multiple of the normal pressure, this constant being the average coefficient of friction and in this analysis this has been obtained from Al-Salehi's[25] experimental results for aluminium and copper and from Shida etal [26] for steel. The deformation

of the plate is analyzed by the rigid-plastic finite element technique coupled with the direct penalty method and Eulerian formulation. An endeavour is made in the analysis to illustrate the effect of strain hardening on the important parameters of roll force,roll torque and the normal pressure distribution which are of utmost importance in the mill design. The reasonably good correlation between experimental results [25,26] and theoretical results over a range of input parameters shows that this model has certain validity and if extended with variable coefficient friction, non-rigid rolls and elastic entry and exit it can produce more accurate results.

1.6. Plan of the Thesis

The thesis is organized as follows.

In the second chapter the mathematical modelling and the Galerkin finite element formulation of the problem of plane-strain cold flat rolling are presented. The application of the boundary equations and the solution procedure are also discussed in this chapter.

In chapter 3 the results obtained by running the model for a range of cases are presented along with the comparison with the experimental results and a discussion on parametric study. A conclusion is drawn and suggestions for further work in the field are given.

CHAPTER 2

MATHEMATICAL MODELLING OF COLD PLANE-STRAIN ROLLING PROCESS

2.1. Introduction

In this chapter the mathematical model for flat cold rolling of plates is developed. Considering that the width of the plate is more than ten times the initial thickness,the process is modelled as a steady state plane-strain problem. The constitutive equations for the mechanical behaviour of the work material are stated. The interaction between the work and its surroundings are represented by appropriate boundary conditions. Non-dimensionalization of governing relations and Galerkin formulation are presented at the end of this chapter.

2.2. Governing equations

The mechanical behavior of the metal is governed by the following two equations.

(1) Conservation of mass or continuity equation :

$$\dot{\rho} + \rho \, \mathrm{div}.\underline{V} = 0 \qquad (2.1)$$

(2) Conservation of momentum or momentum equation :

$$\rho \, \dot{\underline{V}} = \nabla.\underline{\underline{\sigma}} \quad \text{(for zero body forces)} \qquad (2.2)$$

where the dot above $\dot{\underline{V}}$ denotes the material time derivative. The constitutive relations,besides these governing equations,that are used to model the metal behavior are as follows.

In flow formulation the measure of deformation is the rate

of strain tensor, which may mathematically be expressed as

$$\dot{\underline{\underline{\varepsilon}}} = \frac{1}{2}\left[\nabla V + \nabla V^{T}\right] \qquad \text{or} \qquad \dot{\varepsilon}_{ij} = \frac{1}{2}\left(\frac{\partial v_i}{\partial x_j} + \frac{\partial v_j}{\partial x_i}\right) \tag{2.3}$$

In order to express the stress as a function of strain rate in a convenient form the stress and strain rate tensors can be divided into two parts_

$$\underline{\underline{\sigma}} = -p\,\underline{\underline{1}} + \underline{\underline{S}} \quad \text{or} \quad \sigma_{ij} = -p\delta_{ij} + S_{ij} \tag{2.4}$$

where $p=-\frac{1}{3}\mathrm{tr}\,\underline{\underline{\sigma}}$ is the hydrostatic part, $\underline{\underline{S}}$ is the deviatoric part and δ_{ij} is the kronecker delta. Similarly,

$$\dot{\underline{\underline{\varepsilon}}} = \frac{1}{3}\mathrm{tr}\,\dot{\underline{\underline{\varepsilon}}} + \dot{\underline{\underline{\varepsilon}}}' \quad \text{or} \quad \dot{\varepsilon}_{ij} = \frac{1}{3}\dot{\varepsilon}_{kk}\delta_{ij} + \dot{\varepsilon}'_{ij} \tag{2.5}$$

where $\dot{\underline{\underline{\varepsilon}}}'$ is the deviatoric part of the strain-rate tensor. In plastic deformation, since there is no change in volume the hydrostatic part is not related to the deformation. Another consequence of volume constancy is that the hydrostatic part of the strain rate is zero and its deviatoric part is the strain rate tensor itself. Then the deviatoric parts of stress and strain rate tensors can be related as :

$$\underline{\underline{S}} = 2\mu\dot{\underline{\underline{\varepsilon}}} \qquad \text{or} \qquad S_{ij} = 2\mu\dot{\varepsilon}_{ij} \tag{2.6}$$

where 2μ is the proportionality constant. Further if we define the second invariant of deviatoric stress as

$$\bar{S} = \sqrt{\frac{1}{2}S_{ij}S_{ij}} \tag{2.7}$$

and second invariant of strain rate (also known as equivalent

strain rate) as

$$\bar{\dot{\varepsilon}} = \sqrt{2\dot{\varepsilon}_{ij}\dot{\varepsilon}_{ij}} \tag{2.8}$$

then it follows that

$$\bar{S} = \mu\bar{\dot{\varepsilon}}. \tag{2.9}$$

For metals which yield according to von Mises criterion,

$$\bar{S} = \frac{\sigma_y}{\sqrt{3}} \tag{2.10}$$

and μ for such metals comes out to be

$$\mu = \sigma_y / \sqrt{3}\,\bar{\dot{\varepsilon}} \tag{2.11}$$

where σ_y is the yield strength of the metal. In general σ_y may be a function of equivalent strain, temperature and equivalent strain rate. However, if the deformation process is such that the temperature and visco-plastic effects on the mechanical properties can be neglected then it is a function of only equivalent strain.

For a strain hardening metal the yield stress is related to equivalent strain by an equation,

$$\sigma_y = \sigma_o(1+K\bar{\varepsilon})^n \tag{2.12}$$

where σ_o is yield stress of the metal at zero plastic strain and K and n are metal dependent coefficients determined from experiments. The equivalent strain is obtained by time integration of equivalent strain rate as given below:

$$\bar{\varepsilon} = \int_0^t \bar{\dot{\varepsilon}}\, dt \tag{2.13}$$

2.3. Equations for steady-state two-dimensional problem

The work is assumed to be very wide as compared to its thickness and consequently the effect of the spread may be neglected and the problem may be considered as plane-strain. The rolls are assumed to be rigid and the metal is assumed to be rigid-plastic strain hardening yielding according to von Mises criterion. The temperature and visco-plastic effects are neglected because it has been observed that the strain rates in the cases of cold rolling process considered are ignorably small. Only half of the domain is considered for analysis because of symmetry,see figure 2.1, and the rectangular cartesian coordinate system as depicted in figure 2.2 is used.

For plane-strain problem the velocity vector has only two components,

$$\underline{V}=u\hat{i}+v\hat{j} \tag{2.14}$$

while the stress and strain-rate tensors have the following form:

$$\underline{\underline{\sigma}}=\begin{bmatrix} \sigma_{xx} & \sigma_{xy} \\ \sigma_{yx} & \sigma_{yy} \end{bmatrix} \qquad \underline{\underline{\dot{\varepsilon}}}=\begin{bmatrix} \dot{\varepsilon}_{xx} & \dot{\varepsilon}_{xy} \\ \dot{\varepsilon}_{yx} & \dot{\varepsilon}_{yy} \end{bmatrix} \tag{2.15}$$

The process is analyzed at steady state and therefore the governing equations as reduced to 2-D are:

$$\frac{\partial u}{\partial x} + \frac{\partial v}{\partial y}=0 \tag{2.16}$$

$$\left(u\frac{\partial u}{\partial x}+v\frac{\partial u}{\partial y} \right)= - \frac{\partial p}{\partial x} + \frac{\partial S_{xx}}{\partial x} + \frac{\partial S_{xy}}{\partial y} \tag{2.17}$$

$$\left(u\frac{\partial v}{\partial x}+v\frac{\partial v}{\partial y} \right)= - \frac{\partial p}{\partial y} + \frac{\partial S_{yx}}{\partial x} + \frac{\partial S_{yy}}{\partial y} \tag{2.18}$$

where

$$S_{xx}=2\mu\dot{\varepsilon}_{xx}=2\mu\frac{\partial u}{\partial x} \quad ; \quad S_{yy}=2\mu\dot{\varepsilon}_{yy}=2\mu\frac{\partial v}{\partial y} \quad ; \quad S_{xy}=2\mu\dot{\varepsilon}_{xy}=\mu\left(\frac{\partial u}{\partial y}+\frac{\partial v}{\partial x}\right) \qquad (2.19)$$

$$\mu=\sigma_y/(\sqrt{3}\bar{\dot{\varepsilon}}) \qquad (2.20)$$

$$\bar{\dot{\varepsilon}}=\sqrt{2(\dot{\varepsilon}_{xx}^2+\dot{\varepsilon}_{yy}^2+2\dot{\varepsilon}_{xy}^2)} \qquad (2.21)$$

$$\sigma_y=\sigma_o(1+K\bar{\varepsilon})^n \qquad (2.22)$$

2.4. Boundary conditions

The boundary conditions specified on any boundary can be classified as essential boundary conditions i.e., the specification of the velocity vector $\underline{V}$, natural boundary conditions i.e., the specification of the traction vector $\underline{t}=\underline{\underline{\sigma}}.\hat{n}$ or mixed boundary conditions i.e.,specification of one velocity component and one traction component. For the problem under consideration the boundary conditions are as follows(figure 2.3).

(1) Entry and exit boundaries (AF&DE):

The control volume is so selected that its entry and exit boundaries are sufficiently far away from the either side of the deformation zone. This ensures a uniform variation of the velocity before and after deformation and allows the following boundaryconditions for consideration on these regions:

$$\left.\begin{array}{lll} u=U_2 & \text{and} \quad v=0 & \text{on side DE} \\ u=U_1 & \text{and} \quad v=0 & \text{on side AF} \end{array}\right\} \qquad (2.23)$$

i.e., all the material particles on these boundaries have the

prescribed velocities U_1 and U_2 at entry and exit respectively, and the velocities of these particles in Y-direction are zero.

(2) The top free surfaces (AB&CD):

Since these surfaces are traction free,

$$t_x=0 \quad \text{and} \quad t_y=0$$

Also since the flow is only in the X-direction, $v=0$. But only one condition out of the two ($t_y=0, v=0$) has to be chosen. So the final choice of the boundary conditions is

$$t_x=0 \qquad \text{and} \qquad v=0 \tag{2.24}$$

(3) The axis of symmetry(FE):

Because of symmetry, v and t_x are zero on this region of the boundary. Thus

$$v=0 \quad \text{and} \quad t_x=0 \qquad \text{on the axis of symmetry.} \tag{2.25}$$

(4) Work-roll interface (BC):

The component of velocity in the direction normal to the roll-plate interface at any point on the interface is zero.

$$u_n=0 \qquad \text{or} \quad u+v\tan\alpha=0 \tag{2.26}$$

where u and v are the velocities in the directions x and y at any point on the interface and α is the angle made by the unit normal to the interface at that point with the y-axis. At the first contact point on the interface towards entry the angle α is equal to the angle of bite.

The complex and important part of the analysis of rolling process is the treatment of the work-roll interface friction and modelling of the neutral point phenomenon. Many researchers have tried to tackle this problem by using rather arbitrary functional

relations for shear stress in such a way that the position of neutral point is constrained to be within the inlet and exit of the interface, in accordance with the experimental findings. According to Al-Salehi etal,[25] the neutral point,such that the coefficient of friction falls to zero and a shear stress reversal occurs,is present in every case and close to the exit plane. However,none of the works has tried to incorporate the experimentally measured coefficient of friction either directly or indirectly. Such an endeavor is made in this analysis and thus the following relation is used:

$$| t_s | = f | t_n | \qquad (2.27)$$

where 'f' is the coefficient of friction. In this analysis an average value of 'f' is used assuming that it remains constant throughout the deformation process. These values for individual cases considered are taken as reported by Al-Salehi etal.

Further the shear stress in the eq. (2.27) is subject to the constraint

$$\text{if} \quad t_s \geq \frac{\sigma_y}{\sqrt{3}} \quad \text{then} \quad t_s = \frac{\sigma_y}{\sqrt{3}}$$

The method of application of this boundary condition is explained later in the next chapter in detail.

2.5. Non-dimensionalization

Non-dimensionalization is usually done to avoid ill-conditioning and numerical difficulties. The non-dimensionalization of all physical quantities using characteristic dimensional quantities is presented in the

following lines:

$$\tilde{x}= \frac{x}{h_2/2} \quad ; \qquad \tilde{y}= \frac{y}{h_2/2} \quad ; \qquad \tilde{u}=-\frac{u}{U_2} \quad ; \qquad \tilde{v}=-\frac{v}{U_2} \tag{2.28}$$

If we use

$$\mu_o= \frac{\sigma_o}{\sqrt{3}(2\bar{u}_2/h_2)} , \tag{2.29}$$

to non-dimensionalize μ then the expression for $\tilde{\mu}$ may be written as,

$$\tilde{\mu}= \frac{\mu}{\mu_o} = \left(\frac{\sigma_y}{\sigma_o} \right)^{1/\tilde{\dot{\varepsilon}}} \tag{2.30}$$

where the non-dimensionalized strain rate invariant is given by

$$\tilde{\dot{\varepsilon}} = \frac{\bar{\dot{\varepsilon}}}{2\bar{u}_2/h_2} \tag{2.31}$$

For a perfectly plastic material

$$\tilde{\mu} = 1/\tilde{\dot{\varepsilon}} \tag{2.32}$$

The non-dimensionalization of the other quantities is as follows:

$$\left.\begin{aligned} \tilde{p}= \frac{p}{\mu_o 2\bar{u}_2/h_2}=\frac{p}{\sigma_o/\sqrt{3}} \quad ; \quad \tilde{S}_{xx}=\frac{S_{xx}}{\mu_o 2\bar{u}_2/h_2}=\frac{S_{xx}}{\sigma_o/\sqrt{3}} \\ \tilde{S}_{xy}=\frac{S_{xy}}{\mu_o 2\bar{u}_2/h_2}=\frac{S_{xy}}{\sigma_o/\sqrt{3}} \quad ; \quad \tilde{S}_{yy}=\frac{S_{yy}}{\mu_o 2\bar{u}_2/h_2}=\frac{S_{yy}}{\sigma_o/\sqrt{3}} \end{aligned}\right\} \tag{2.33}$$

The non-dimensionalization of the continuity and momentum

equations is obtained by substituting the eqs.(2.28) to (2.33) in eqs.(2.16) to (2.18) .

$$\frac{\partial \tilde{u}}{\partial \tilde{x}}+\frac{\partial \tilde{v}}{\partial \tilde{y}}=0 \tag{2.34}$$

$$\frac{\rho u_2 h_2}{2\mu_o}\left[\tilde{u}\frac{\partial \tilde{u}}{\partial \tilde{x}}+\tilde{v}\frac{\partial \tilde{u}}{\partial \tilde{y}}\right]+\frac{\partial \tilde{p}}{\partial \tilde{x}}-\left[\frac{\partial \tilde{S}_{xx}}{\partial \tilde{x}}+\frac{\partial \tilde{S}_{xy}}{\partial \tilde{y}}\right]=0 \tag{2.35}$$

similarly,

$$\frac{\rho u_2 h_2}{2\mu_o}\left[\tilde{u}\frac{\partial \tilde{v}}{\partial \tilde{x}}+\tilde{v}\frac{\partial \tilde{v}}{\partial \tilde{y}}\right]+\frac{\partial \tilde{p}}{\partial \tilde{y}}-\left[\frac{\partial \tilde{S}_{yx}}{\partial \tilde{x}}+\frac{\partial \tilde{S}_{yy}}{\partial \tilde{y}}\right]=0 \tag{2.36}$$

Since the Reynolds number $\left(\frac{\rho u_2 h_2}{2\mu_o}\right)$ is found to be typically of the order of 10^{-8} for all the cases considered, the inertial terms may be ignored. Thus the summarised non-dimensional forms of the continuity and momentum equations are:

$$\frac{\partial \tilde{u}}{\partial \tilde{x}}+\frac{\partial \tilde{v}}{\partial \tilde{y}}=0 \tag{2.37}$$

$$-\frac{\partial \tilde{p}}{\partial \tilde{x}}+\left[\frac{\partial \tilde{S}_{xx}}{\partial \tilde{x}}+\frac{\partial \tilde{S}_{xy}}{\partial \tilde{y}}\right]=0 \tag{2.38}$$

$$-\frac{\partial \tilde{p}}{\partial \tilde{y}}+\left[\frac{\partial \tilde{S}_{yx}}{\partial \tilde{x}}+\frac{\partial \tilde{S}_{yy}}{\partial \tilde{y}}\right]=0 \tag{2.39}$$

2.6. Galerkin Finite Element Formulation

2.6.1.Galerkin Weak Formulation with Direct Penalty Method:

In this analysis the Galerkin weighed residual method coupled with direct penalization is used for the finite element formulation of the governing equations. In the mixed or pressure-velocity formulation where pressure is also a nodal variable, the coefficient matrix becomes a non-positive-definite matrix because of the zeroes appearing along the principal diagonal, therefore entailing a solution method employing complete pivoting. Also since the pressure does not occur as a degree of freedom at every node, the computer implementation of assembly becomes more complicated [27]. To overcome these problems and because of some of the other advantages with direct penalty formulation with reduced integration [28], this method is adopted in the present analysis.

In direct penalty formulation the pressure in the momentum equations is eliminated using the following relationship

$$-\frac{\tilde{p}}{\bar{\lambda}} = -\left[\frac{\partial \tilde{u}}{\partial \tilde{x}} + \frac{\partial \tilde{v}}{\partial \tilde{y}} \right] \qquad (2.40)$$

where

$$\bar{\lambda} = \frac{\lambda}{\mu_o}$$

and λ, which is called the penalty factor, is a very large number. In the limit as $\lambda \to \infty$,equation (2.40) reduces to equation (2.37).The value of λ is usually chosen in such a way that

$$\lambda \leq 10^{13},$$

the upper limit being dependent on the computer.

The weak form is derived in this sub-section and the finite element formulation is presented in the next sub-section. Let $\tilde{u}$ and $\tilde{v}$ be the functions which satisfy all the essential boundary

conditions exactly. Then $\tilde{u}$ and $\tilde{v}$ constitute a weak solution if the following integral equation is satisfied.

$$\int_A \left[\frac{\partial \tilde{p}}{\partial x} w_u + \frac{\partial \tilde{p}}{\partial y} w_v - \left\{ w_u \left(\frac{\partial \tilde{S}_{xx}}{\partial x} + \frac{\partial \tilde{S}_{xy}}{\partial y} \right) + w_v \left(\frac{\partial \tilde{S}_{yx}}{\partial x} + \frac{\partial \tilde{S}_{yy}}{\partial y} \right) \right\} \right] dA = 0 \qquad (2.41)$$

where w_u and w_v are weight functions which satisfy the homogeneous versions of the boundary conditions and 'A' represents the area of the domain.

Performing the above integration by parts the following weak form can be obtained:

$$\int_A \left[-\tilde{p} \left(\frac{\partial w_u}{\partial x} + \frac{\partial w_v}{\partial y} \right) + \left(\tilde{S}_{xx} \frac{\partial w_u}{\partial x} + \tilde{S}_{xy} \left[\frac{\partial w_u}{\partial y} + \frac{\partial w_v}{\partial x} \right] + \tilde{S}_{yy} \frac{\partial w_v}{\partial y} \right) \right] dA -$$

$$\int_\Gamma \left[\left(w_u \tilde{S}_{xx} n_x + w_u \tilde{S}_{xy} n_y + w_v \tilde{S}_{yx} n_x + w_v \tilde{S}_{yy} n_y \right) - \left(w_u \tilde{p} n_x + w_v \tilde{p} n_y \right) \right] d\Gamma = 0 \qquad (2.42)$$

where Γ represents the boundary of the entire domain under consideration.

Substituting for $\tilde{p}$ from eq. (2.40) and for S_{ij} form eq. (2.19) only in the area integral, the relation in eq. (2.4) only in the boundary integral and using the relation

$$\begin{Bmatrix} t_x \\ t_y \end{Bmatrix} = \begin{bmatrix} \sigma_{xx} & \sigma_{xy} \\ \sigma_{yx} & \sigma_{yy} \end{bmatrix} \begin{Bmatrix} n_x \\ n_y \end{Bmatrix} \qquad (2.43)$$

we obtain the final weak form as

$$\int_A \left[\bar{\lambda} \left(\frac{\partial \tilde{u}}{\partial \tilde{x}} + \frac{\partial \tilde{v}}{\partial \tilde{y}} \right) \left(\frac{\partial w_u}{\partial \tilde{x}} + \frac{\partial w_v}{\partial \tilde{y}} \right) + 2\tilde{\mu} \left(\tilde{\dot{\varepsilon}}_{xx} \frac{\partial w_u}{\partial \tilde{x}} + \tilde{\dot{\varepsilon}}_{xy} \left(\frac{\partial w_u}{\partial \tilde{y}} + \frac{\partial w_v}{\partial \tilde{x}} \right) + \tilde{\dot{\varepsilon}}_{yy} \frac{\partial w_v}{\partial \tilde{y}} \right) \right] dA$$

$$- \int_\Gamma \left(t_x w_u + t_y w_v \right) d\Gamma = 0 \qquad (2.44)$$

2.6.2 Finite Element Approximation:

In contrast to the traditional Galerkin-Weighed Residual Method where a global approximation is chosen for the field variable, in finite element method the domain is discretized into small elements and the above integral is evaluated over each element after suitably selecting the approximation for the field variable over each element. Then the elemental expressions are assembled to yield the global FEM expression.

The eq. (2.44) suggests that the convergence criteria will be satisfied if $\tilde{u}$ and $\tilde{v}$ are chosen to be bilinear functions of $\tilde{x}$ and $\tilde{y}$. So one can use bilinear interpolation for $\tilde{u}$ and $\tilde{v}$. However,higher polynomials give better results. We choose nine-noded Lagrangian element and corresponding biquadratic nodal shape functions for $\tilde{u}$ and $\tilde{v}$, figure 2.4.

The approximation for $\tilde{u}$ and $\tilde{v}$ is as follows:

$$\begin{Bmatrix} \tilde{u} \\ \tilde{v} \end{Bmatrix} = \begin{bmatrix} N_1 & 0 & N_2 & 0 & \cdots\cdots\cdots & N_9 & 0 \\ 0 & N_1 & 0 & N_2 & \cdots\cdots\cdots & 0 & N_9 \end{bmatrix} \begin{Bmatrix} \tilde{u}_1^e \\ \tilde{v}_1^e \\ \vdots \\ \tilde{u}_9^e \\ \tilde{v}_9^e \end{Bmatrix} \qquad (2.45)$$

i.e., $[\tilde{V}] = [N_v][\tilde{V}^e]$

In Galerkin formulation the weight functions are approximated using the shape functions as that for velocity.

$$[W] = \begin{Bmatrix} w_u \\ w_v \end{Bmatrix} = [N_v][W^e] \qquad (2.46)$$

The vectors $[\tilde{V}^e]$ and $[W^e]$ respectively contain the velocities at the nodes of elements and their corresponding weight functions.

The expressions for the shape functions for nine noded Lagrangian quadratic rectangular element are given by:

$$\left.\begin{aligned} N_1 &= \tfrac{1}{4}(\xi^2-\xi)(\eta^2-\eta) \;;\; N_2 = \tfrac{1}{4}(\xi^2+\xi)(\eta^2-\eta) \;;\; N_3 = \tfrac{1}{4}(\xi^2+\xi)(\eta^2+\eta) \\ N_4 &= \tfrac{1}{4}(\xi^2-\xi)(\eta^2+\eta) \;;\; N_5 = \tfrac{1}{2}(1-\xi^2)(\eta^2-\eta) \;;\; N_6 = \tfrac{1}{2}(\xi^2+\xi)(1-\eta^2) \\ N_7 &= \tfrac{1}{2}(1-\xi^2)(\eta^2+\eta) \;;\; N_8 = \tfrac{1}{2}(\xi^2-\xi)(1-\eta^2) \;;\; N_9 = (1-\xi^2)(1-\eta^2) \end{aligned}\right\} \qquad (2.47)$$

where ξ and η are the local coordinates and are related to the global coordinates $\tilde{x}$ and $\tilde{y}$ with subparametric formulation as follows:

$$\tilde{x}=\sum_{i=1}^{4}\tilde{x}_i N_i \qquad \tilde{y}=\sum_{i=1}^{4}\tilde{y}_i N_i \tag{2.48}$$

where

$$\left.\begin{aligned} N_1&=\tfrac{1}{4}(1-\xi)(1-\eta) & N_2&=\tfrac{1}{4}(1+\xi)(1-\eta)\\ N_3&=\tfrac{1}{4}(1-\xi)(1+\eta) & N_4&=\tfrac{1}{4}(1+\xi)(1+\eta)\end{aligned}\right\} \tag{2.49}$$

The boundary approximation, figure 2.5, is made consistent with the area approximation as follows.

$$\begin{Bmatrix} w_u \\ w_v \end{Bmatrix} = \begin{bmatrix} N_1 & 0 & N_2 & 0 & N_3 & 0 \\ 0 & N_1 & 0 & N_2 & 0 & N_3 \end{bmatrix} \begin{bmatrix} w_{u_1}^{be} \\ w_{v_1}^{be} \\ \vdots \\ w_{u_3}^{be} \\ w_{v_3}^{be} \end{bmatrix} = [N_b][W_b^{be}] \tag{2.50}$$

where $[N_b]$ is the vector of Lagrangian quadratic shape functions and $[W_b^{be}]$ is the vector of local boundary weight functions for a typical - boundary element. Further we approximate t_x and t_y as,

$$\begin{Bmatrix} \tilde{t}_x \\ \tilde{t}_y \end{Bmatrix} = \begin{bmatrix} N_1 & 0 & N_2 & 0 & N_3 & 0 \\ 0 & N_1 & 0 & N_2 & 0 & N_3 \end{bmatrix} \begin{bmatrix} \tilde{t}_{x_1}^{be} \\ \tilde{t}_{y_1}^{be} \\ \vdots \\ \tilde{t}_{x_3}^{be} \\ \tilde{t}_{y_3}^{be} \end{bmatrix} = [N_b]\{\tilde{t}_b^{be}\} \tag{2.51}$$

where $\{t_b^{be}\}$ is the vector of local boundary tractions for a typical boundary element.

2.7. Finite Element Equations in Local Variables

The following definitions of some vectors should precede the presentation of elemental expressions and their assembly, for compactness and ease of understanding.

The strain-rate vector is defines as follows.

$$\underset{\sim}{\dot{\varepsilon}} = \begin{bmatrix} \tilde{\dot{\varepsilon}}_{xx} \\ \tilde{\dot{\varepsilon}}_{yy} \\ \sqrt{2}\ \tilde{\dot{\varepsilon}}_{xy} \end{bmatrix} \tag{2.52}$$

or further

$$= \begin{bmatrix} \dfrac{\partial \tilde{u}}{\partial \tilde{x}} \\ \dfrac{\partial \tilde{v}}{\partial \tilde{y}} \\ \dfrac{1}{\sqrt{2}}\left(\dfrac{\partial \tilde{u}}{\partial \tilde{y}} + \dfrac{\partial \tilde{v}}{\partial \tilde{x}}\right) \end{bmatrix} = [\ B\ ]\ [\ \tilde{V}^e] \tag{2.53}$$

and

$$\begin{bmatrix} \frac{\partial w_u}{\partial \tilde{x}} \\ \frac{\partial w_v}{\partial \tilde{y}} \\ \frac{1}{\sqrt{2}}\left(\frac{\partial w_u}{\partial \tilde{y}} + \frac{\partial w_v}{\partial \tilde{x}}\right) \end{bmatrix} = [\,B\,]\,[\,w^e] \qquad (2.54)$$

where

$$[\,B\,] = \begin{bmatrix} \frac{\partial N_1}{\partial \tilde{x}} & 0 & \frac{\partial N_2}{\partial \tilde{x}} & 0 & \cdots & \frac{\partial N_9}{\partial \tilde{x}} & 0 \\ 0 & \frac{\partial N_1}{\partial \tilde{y}} & 0 & \frac{\partial N_2}{\partial \tilde{y}} & \cdots & 0 & \frac{\partial N_9}{\partial \tilde{y}} \\ \frac{1}{\sqrt{2}}\frac{\partial N_1}{\partial \tilde{y}} & \frac{1}{\sqrt{2}}\frac{\partial N_1}{\partial \tilde{x}} & \frac{1}{\sqrt{2}}\frac{\partial N_2}{\partial \tilde{y}} & \frac{1}{\sqrt{2}}\frac{\partial N_2}{\partial \tilde{x}} & \cdots & \frac{1}{\sqrt{2}}\frac{\partial N_9}{\partial \tilde{y}} & \frac{1}{\sqrt{2}}\frac{\partial N_9}{\partial \tilde{x}} \end{bmatrix} \qquad (2.55)$$

Substituting the the area elemental approximation from eq. (2.45) to eq. (2.49) in the area terms of eq. (2.44) and noting that

$$\frac{\partial \tilde{u}}{\partial \tilde{x}} + \frac{\partial \tilde{v}}{\partial \tilde{y}} = [\,m\,]^T [\,B\,][\,\tilde{v}^e] \quad \text{and} \quad \frac{\partial w_u}{\partial \tilde{x}} + \frac{\partial w_v}{\partial \tilde{y}} = [\,w^e][\,B\,][\,m\,]$$

where $[\,m\,] = \begin{bmatrix} 1 \\ 1 \\ 0 \end{bmatrix}$,

we obtain the elemental area term in matrix form as

$$\int_{A^e}\left[\frac{\lambda}{\tilde{\mu}_o}\left\{[W^e][B]^T[m][m]^T[B][\tilde{V}^e]\right\}+\right.$$

$$\left.\left\{2\tilde{\mu}[W^e]^T[B]^T[B][\tilde{V}^e]\right\}\right]dA^e \qquad (2.56)$$

Further substituting the boundary approximation from eqs. (2.50) and (2.51) in the boundary term of eq. (2.44) we obtain the elemental boundary term as

$$\int_{\Gamma^e}[W_b^{be}]^T[N_b]^T[N_b]\{\tilde{t}_b^{be}\}\,d\Gamma^e \qquad (2.57)$$

To convert the above integral equations from the global coordinates to local coordinates, $\tilde{x}$ and $\tilde{y}$ are to be changed to ξ and η using the following relation.

$$\int(....)\,d\tilde{x}\,d\tilde{y} = \int_{-1}^{+1}\int_{-1}^{+1}(....)|J|\,d\xi\,d\eta \qquad (2.58)$$

where $|J|$, the jacobian, is the determinant of the jacobian matrix,

$$\begin{bmatrix} \frac{\partial\tilde{x}}{\partial\xi} & \frac{\partial\tilde{x}}{\partial\eta} \\ \frac{\partial\tilde{y}}{\partial\xi} & \frac{\partial\tilde{y}}{\partial\eta} \end{bmatrix}$$

Thus the eq. (2.56) and eq. (2.57) can be written in terms of natural coordinates as

$$\int_{-1}^{+1}\int_{-1}^{+1}\left[\frac{\lambda}{\mu_o}\left\{[W^e][B]^T[m][m]^T[B][\tilde{V}^e]\right\}|J|\,d\xi\,d\eta + \int_{-1}^{+1}\int_{-1}^{+1}\left\{2\tilde{\mu}[W^e]^T[B]^T[B][\tilde{V}^e]\right\}\right]|J|\,d\xi\,d\eta \tag{2.59}$$

and

$$\int_{-1}^{+1}[W_b^{be}]^T[N_b]^T[N_b]\{\tilde{t}_b^{be}\}|J_b|\,d\zeta \tag{2.60}$$

respectively where $|J|$ is the jacobian for the area terms and $|J_b|$ is the jacobian for the boundary term and ζ is the natural coordinate for the boundary linear elements.

2.8 Global Assembly

The final finite element equation is obtained by assembling the elemental area and boundary matrices into global area and boundary terms,respectively, and then equating as follows.

$$\sum_{e=1}^{nelem}\left[\frac{\lambda}{\mu_o}\int_{-1}^{+1}\int_{-1}^{+1}\left\{[W^e][B]^T[m][m]^T[B][\tilde{V}^e]\right\}|J|\,d\xi\,d\eta+\right.$$

$$\left.\int_{-1}^{+1}\int_{-1}^{+1}\left\{2\tilde{\mu}[W^e]^T[B]^T[B][\tilde{V}^e]\right\}|J|\,d\xi\,d\eta\right]$$

$$=\sum_{be=1}^{nbelem}\left[\int_{-1}^{+1}[W_b^{be}]^T[N_b]^T[N_b]\{\tilde{t}_b^{be}\}\,|J_b|\,d\zeta\right] \tag{2.61}$$

Further it can also be written as

$$\sum_{e=1}^{nelem}\left[[W_v^e]^T[k^e][\tilde{V}^e]\right]=\sum_{be=1}^{nbelem}\left[[W_b^{be}]^T[f_b^{be}]\right] \tag{2.62}$$

where

$$[k^e]=[k^e]_1+\bar{\lambda}[k^e]_2 \tag{2.63}$$

$$[k^e]_1=\int_{-1}^{+1}\int_{-1}^{+1}\left\{2\tilde{\mu}[B]^T[B]\right\}|J|\,d\xi\,d\eta \tag{2.64}$$

$$[k^e]_2=\int_{-1}^{+1}\int_{-1}^{+1}\left\{[B]^T[m][m]^T[B]\right\}|J|\,d\xi\,d\eta \tag{2.65}$$

$$[f_b^{be}]=\int_{-1}^{+1}\left\{[N_b]^T[N_b]\{\tilde{t}_b^{be}\}\right\}|J_b|\,d\zeta \tag{2.66}$$

The elemental area matrix $[k^e]$ is prepared by evaluating the integral by reduced integration technique where $[k^e]_1$ is integrated by 3*3 gauss quadrature and $[k^e]_2$ by 2*2 gauss quadrature. This ensures that $[k^e]_2$ is singular so that even for fairly large values of λ,the penalty factor,a non-trivial solution may be obtained.

The assembly of the elemental area matrices into the global area matrix is done by transferring the elements corresponding to a local degree of freedom in each elemental area matrix to positions of corresponding global degrees of freedom in the global area matrix. Similar procedure is followed for the assembly of global boundary matrix. The assembled finite element equation may be written as

$$[\,W\,]^T[\,K\,][\,V\,] = [\,W\,]^T[\,F\,] \qquad (2.67)$$

where $[\,W\,]$ contains global nodal weight functions, $[\,K\,]$ is the global stiffness matrix, $[\,V\,]$ contains the global nodal velocities and $[\,F\,]$ is the global load matrix.

Since $[\,W\,]$ is arbitrary we can eliminate it from both sides and thus we obtain the final general equation of FEM,

$$[\,K\,][\,V\,] = [\,F\,] \qquad (2.68)$$

2.9. Application of Boundary conditions

The application of natural and essential boundary conditions is done as follows.

The natural boundary condition on the work-roll interface can be applied without requiring to evaluate the matrix $[f_b^{be}]$ in the

following manner (figure 2.6).

Let us consider a typical boundary element 'j' on the work piece-roll interface. The elemental boundary matrix for this element would be as given by eq. (2.66). At a middle node 'i' of this boundary element 'j', whose corresponding global node number is 'k', we can write the contribution of this node to the local boundary matrix and there by to the global load matrix as follows.

$$[F]_{2k-1}=[f_b^j]_{2i-1}=\left(\int_{-1}^{+1}[N_b]^T[N_b]|J_b|\,d\zeta\,\{\tilde{t}_b^j\}\right)_{2i-1} \quad \text{and}$$

$$[F]_{2k}=[f_b^j]_{2i}=\left(\int_{-1}^{+1}[N_b]^T[N_b]|J_b|\,d\zeta\,\{\tilde{t}_b^j\}\right)_{2i}$$

where $[F]_{2k-1}$ and $[F]_{2k}$ are the elements of the global load matrix containing the odd and even net force contributions from the global boundary node 'k', respectively. Now for this node the relation in equation eq. (2.27) can be written as

$$|\tilde{t}_s|_k=f|\tilde{t}_n|_k$$

$$\text{or} \qquad (\tilde{t}_s)_k=fk_s(\tilde{t}_n)_k \qquad \text{where} \qquad k_s=\frac{\text{sign of } \tilde{t}_s}{\text{sign of } \tilde{t}_n}$$

Writing $(\tilde{t}_s)_k$ and $(\tilde{t}_n)_k$ in terms of $(\tilde{t}_x)_k$ and $(\tilde{t}_y)_k$ (figure 2.6),

$$[(\tilde{t}_x)_k\cos\alpha_k-(\tilde{t}_y)_k\sin\alpha_k]=fk_s[(\tilde{t}_y)_k\cos\alpha_k+(\tilde{t}_x)_k\sin\alpha_k]$$

where α_k is the value of α at the global node 'k'.

$$(\tilde{t}_x)_k[\cos\alpha_k-fk_s\sin\alpha_k]=(\tilde{t}_y)_k[\sin\alpha_k+fk_s\cos\alpha_k].$$

Converting the $(\tilde{t}_x)_k$ and $(\tilde{t}_y)_k$ into matrices analogous to, but 1 - D, boundary elemental traction matrix and multiplying both sides with

$$\int_{-1}^{+1} [N_b^1]^T [N_b^1] |J_b| \, d\zeta \quad \text{where} \quad [N_b^1] = [N_1 \;\; N_2 \;\; N_3] \tag{2.68}$$

and replacing $(\tilde{t}_x)_k$ and $(\tilde{t}_y)_k$ with $\{\tilde{t}_b^j\}_{2i-1}$ and $\{\tilde{t}_b^j\}_{2i}$ respectively, the following expression is obtained_

$$\left(\int_{-1}^{+1} [N_b]^T [N_b] |J_b| \, d\zeta \, \{\tilde{t}_b^j\} \right)_{2i-1} [\cos\alpha_k - fk_s \sin\alpha_k]$$

$$= \left(\int_{-1}^{+1} [N_b]^T [N_b] |J_b| \, d\zeta \, \{\tilde{t}_b^j\} \right)_{2i} [\sin\alpha_k + fk_s \cos\alpha_k]$$

This gives the contribution of one node of the element 'j'. Since α does not vary much from one local node to other in an element, similar evaluation for other two nodes and then summation over all three nodes of the element gives

$$[f_b^j]_{2i-1} [\cos\alpha_k - fk_s \sin\alpha_k] = [f_b^j]_{2i} [\sin\alpha_k + fk_s \cos\alpha_k] .$$

Further

$$[F]_{2k-1} [\cos\alpha_k - fk_s \sin\alpha_k] = [F]_{2k} [\sin\alpha_k + fk_s \cos\alpha_k]$$

Thus instead of evaluating $[F]_{2k-1}$ and $[F]_{2k}$ for any typical global interface node k, we perform the following the matrix operations in order to apply this natural boundary condition.

For each boundary node 'k' on the interface,

(i) replace each element of (2k-1)th row of global stiffness matrix by:

[element of (2k-1)th row $\otimes$ ($\cos\alpha_k - fk_s \sin\alpha_k$)-

element of (2k)th row in the same column $\otimes$ ($\sin\alpha_k + fk_s \cos\alpha_k$)]

(ii) replace (2k-1)th element in global load matrix by zero.

The boundary condition expressed in eq. (2.26) at a typical global node 'i' is applied through the following steps.

(i) Replace all the elements of (2k)th row of the global stiffness matrix and that in the global load matrix by zeroes.

(ii) Substitute '1' in the elemental position of (2k)th row and (2k-1)th column, and the value of $\tan\alpha$, evaluated with α at node 'i' in the elemental position of (2k)th row and (2k)th column of the global stiffness matrix.

2.10. Formulation for Strain Hardening

The equivalent strain may be obtained by the time integration of equivalent strain rates as,

$$\bar{\varepsilon} = \frac{1}{\sqrt{3}} \int \bar{\dot{\varepsilon}}\, dt \qquad (2.72)$$

where $\bar{\varepsilon}$ and $\bar{\dot{\varepsilon}}$ are the equivalent strain and strain rates respectively and the factor $\frac{1}{\sqrt{3}}$ is introduced so that the equivalent strain is equivalent to the axial strain in a tensile test. Differentiation of the above equation leads to

$$\frac{d\bar{\varepsilon}}{dt} = \frac{1}{\sqrt{3}} \bar{\dot{\varepsilon}} \qquad (2.73)$$

where $\frac{d}{dt}$ is the material time derivative as it is in Eulerian formulation. For 2-D steady state case, as ours, the above equation can be written in non-dimensionalized form as

$$\tilde{u} \frac{\partial \bar{\varepsilon}}{\partial \tilde{x}} + \tilde{v} \frac{\partial \bar{\varepsilon}}{\partial \tilde{y}} = \frac{1}{\sqrt{3}} \tilde{\bar{\dot{\varepsilon}}} \qquad (2.74)$$

This equation has to be solved along with the condition $\bar{\varepsilon}=0$ at the inlet.

Galerkin formulation of the above equation over an element gives the following integral:

$$\int_{A^e}\int\left[\left(\tilde{u}\frac{\partial\bar{\varepsilon}}{\partial\tilde{x}}+\tilde{v}\frac{\partial\bar{\varepsilon}}{\partial\tilde{y}}\right)w_s-\sqrt{\frac{1}{3}}w_s\dot{\bar{\varepsilon}}\right]\,dx\,dy=0 \qquad (2.75)$$

where w_s is the weight function.

The integral may be expressed in matrix form as given below.

$$\int_{A^e}\left[\,w_s\,[\,\tilde{u}\quad\tilde{v}]\begin{bmatrix}\frac{\partial\bar{\varepsilon}}{\partial\tilde{x}}\\ \frac{\partial\bar{\varepsilon}}{\partial\tilde{y}}\end{bmatrix}-w_s\sqrt{\frac{1}{3}}\;\dot{\bar{\varepsilon}}\,\right]dx\,dy=0 \qquad (2.76)$$

In the finite element approximation for equivalent strains and the weight function the same shape functions as used in the velocity approximation are used.

$$\bar{\varepsilon}=\sum_1^9 N_i\bar{\varepsilon}_i=\{N^1\}^T\{\bar{\varepsilon}^e\}\qquad w_s=\sum_1^9 N_i(w_s)_i=\{N^1\}\{w_s^e\} \qquad (2.77)$$

where $\{N\}$ is the 1-D array of quadratic shape functions as defined below,

$$\{N^1\}=[N_1\quad N_2\ \ldots\ldots\ldots N_9] \qquad (2.78)$$

and the differentiation of strains in equation (2.77) leads to

$$\begin{bmatrix} \frac{\partial \bar{\varepsilon}}{\partial \tilde{x}} \\ \frac{\partial \bar{\varepsilon}}{\partial \tilde{y}} \end{bmatrix} = [\, H \,]\{\, \bar{\varepsilon}^{e}\} \tag{2.79}$$

where $[\, H \,]$ is defined as given below.

$$[\, H \,] = \begin{bmatrix} \frac{\partial N_1}{\partial \tilde{x}} & 0 & \frac{\partial N_2}{\partial \tilde{x}} & 0 & \cdots & \frac{\partial N_9}{\partial \tilde{x}} & 0 \\ 0 & \frac{\partial N_1}{\partial \tilde{y}} & 0 & \frac{\partial N_2}{\partial \tilde{y}} & \cdots & 0 & \frac{\partial N_9}{\partial \tilde{y}} \end{bmatrix} \tag{2.80}$$

Substituting the approximation for equivalent strain ,weight function and velocities in eqs. (2.77) and (2.45) we obtain the following integral equation.

$$\sum_{e=1}^{nelem} \left[\int_{A^e} \left\{ [\, w_g^e]^T [\, N^1]^T [\, \tilde{V}^e]^T [\, N_v]^T [\, H \,]\{\, \bar{\varepsilon}^e\} \right\} dx\, dy - \sqrt{\frac{1}{3}} \int_{A^e} \left([\, w_S^e]^T [N^1]^T \tilde{\bar{\varepsilon}} \right) dx\, dy \right] = 0 \tag{2.81}$$

To facilitate the numerical integration, the variables are changed to the natural coordinates. The final expression can be obtained as

$$[\, W_g]^T \left[\sum_{e=1}^{nelem} \left([\, k_g^e] \right) \{\, \bar{\varepsilon}\,\}^T = \sum_{e=1}^{nelem} \left([\, r^e] \right) \right] \tag{2.82}$$

where

$$[k_s^e] = \int_{-1}^{+1}\int_{-1}^{+1} \left\{ [N^1]^T [\tilde{V}^e]^T [N_v]^T [H] \right\} |J| \, d\xi \, d\eta \qquad (2.83)$$

is the elemental coefficient matrix for the evaluation of equivalent strains and

$$[r^e] = \frac{1}{\sqrt{3}} \int_{-1}^{+1}\int_{-1}^{+1} \left([N^1]^T \tilde{\bar{\dot{\varepsilon}}} \right) |J| \, d\xi \, d\eta \qquad (2.84)$$

is the elemental right side vector. Since $[W_s]^T$ is arbitrary, we obtain the following equation in terms of global matrices,

$$[K_s]\{\bar{\varepsilon}\} = [R] \qquad (2.85)$$

where the $[K_s]$ is the global coefficient matrix, $\{\bar{\varepsilon}\}$ is the global nodal equivalent strains matrix and $[R]$ is the global right hand side, for the evaluation of equivalent strains. In equation (2.84) $\tilde{\bar{\dot{\varepsilon}}}$ is the non-dimensional equivalent strain-rate which may directly be obtained at each gauss-point from the velocity field of previous iteration.

2.11. Implementation

While correct modelling of the physical problem into a mathematical equation forms the core of the entire analysis, selection of degree of refinement of mesh, value of the penalty factor, the convergence criteria, the threshold value of $\tilde{\mu}$ and other mesh related parameters decides the achievement of

reasonable results. It has been experienced that the judgment about the later mentioned selection of various parameters needs a wide knowledge of capabilities and liabilities of computers as well it entails a good deal of numerical experiments before a particular set of values is used for final results. A brief discussion is presented in the following lines about some of these factors.

The length of the inlet and exit zones is usually taken as follows:

$$l_i = nh_1/2 \qquad \text{and} \qquad l_o = nh_2/2$$

where l_i and l_o are the inlet and exit zone lengths respectively, 'n' is a multiplying factor and h_1, h_2 are the inlet and exit thicknesses of the plate. The value for 'n' has to be selected such that uniform conditions prevail at the beginning of the inlet zone and end of the exit. A value of 6 has been selected in this analysis after conducting a few numerical experiments.

The value of penalty factor λ is usually selected as per the directions given elsewhere in this chapter. For this analysis λ is found as follows:

$$\lambda = \tilde{\lambda}\mu_o$$

where $\tilde{\lambda}$ is a numerical value in the range 10^2 to 10^5. Although the pressure remains fairly unaltered for a reasonably wide range of values of λ, very high values may render the solution to be spurious. A value of $\tilde{\lambda}=10^3$ has been chosen in this analysis and used constantly for all the cases.

In this analysis of rolling the neutral point is not known a priori. Therefore, for the first iteration an approximate neutral point is determined by the following Avitzur's analytical formula:

$$\alpha_n = \frac{1}{3}\sqrt{\frac{R}{h_2}}\left[\tan^{-1}\sqrt{\frac{h_1}{h_2}-1} - \frac{1}{m}\sqrt{\frac{h_2}{R}}\left\{\ln\left[\frac{h_1}{h_2}\right]+\frac{1}{4}\sqrt{\frac{h_2}{R}}\left[\frac{h_1}{h_2}-1\right] + \frac{\sigma_{xb}-\sigma_{xf}}{(2/\sqrt{3})\sigma_o}\right\}\right]$$

where

α_n = the neutral angle

R = roll radius

h_1, h_2 = the initial and final thicknesses of the plate

m = the friction factor

σ_{xb}, σ_{xf} = the back and front tensions respectively

σ_o = the initial yield stress of the metal

Thus the relative signs k_s at each interface node is determined as follows:

$\tilde{t}_s$ is (+) ve in the backward slip zone
$\tilde{t}_n$ is (-) ve in the backward slip zone
} k_s is (-) in the backward slip zone

$\tilde{t}_s$ is (-) ve in the forward slip zone
$\tilde{t}_n$ is (-) ve in the forward slip zone
} k_s is (-) in the forward slip zone

This approximation is used only for the first iteration and the second iteration onwards the relative signs are determined from the computations of $\tilde{t}_s$ and $\tilde{t}_n$ from the solution of the immediately preceding iteration (the computation of $\tilde{t}_s$

and $\tilde{\tau}_n$ is explained later).

The strategy followed for obtaining the converged solution with and without strain hardening is as follows. First a converged solution (nodal velocities) without strain hardening has been obtained. For this portion of the analysis the $\tilde{\mu}$ is simply as given in the eq. (2.32). This solution is then used as the initial solution for the further analysis and the yield strength is updated by evaluating strains from immediately preceding solution in every successive iteration. Thus the value of $\tilde{\mu}$ is evaluated from the eq. (2.31).

Preliminary runs have been conducted with coarser mesh using various solution algorithms viz. gauss elimination method, IMSL routine with and without iterative solving, NAG routine etc. on the HP super mini computer to check the validity of our gauss elimination subroutine. Then final runs with refined mesh are conducted on CONVEX mini super computer to harness the high speed parallel computing using this solution routine. Because of the assumption of rigid portions in the inlet and exit zones, the high value of $\tilde{\mu}$ renders the coefficient matrix to be ill-conditioned, especially during strain hardening because the $\tilde{\mu}$ is updated. To counter this problem, $\tilde{\mu}$ is to be restricted to a threshold minimum, which is equal to the reciprocal of set off value of non-dimensional equivalent strain-rate.

The convergence criteria used for velocity are as follows. All values of velocities less than 10^{-4} are considered to be equal to zero and are not checked for convergence. A percentage difference less than 10^{-4} for u-velocities and 10^{-2} for

v-velocities between solutions of two successive iterations is considered to mark the convergence of the solution , i.e., nodal velocities. This is done because the v-velocities are about two orders magnitude smaller than u-velocities.

2.12. Evaluation of the Secondary Quantities

As explained above the solution to the problem is obtained in the form of nodal velocities. Thereby the secondary quantities viz. strain rates, deviatoric stresses, hydrostatic pressure and interface boundary tractions are evaluated in each iteration to determine the non-linear parameters like $\tilde{\mu}$,k_s etc.,as well as at the end from the final converged solution for parametric study. The details of these calculations are explained in the following lines briefly.

(i) The Hydrostatic Pressure at Gauss Points:

The pressure at the gauss points is post-evaluated from the Lagrangian multiplier as follows:

$$\tilde{p}=-\tilde{\lambda}\left(\frac{\partial\tilde{u}}{\partial\tilde{x}}+\frac{\partial\tilde{v}}{\partial\tilde{y}} \right) = - \tilde{\lambda} \{ m \}^T [B] \{ \tilde{V}^e \}$$

This is evaluated at 2x2 gauss points.

(ii) Interface Boundary Tractions:

Just like pressure the strain rates and the total stresses are also evaluated at 2x2 gauss points. The reciprocal of the non-dimensional strain-rate invariant helps in calculation of $\tilde{\mu}$. The stresses at gauss points are linearly extrapolated on to the boundary nodes in a few steps. Then the tangential and normal tractions are evaluated at each interface node using the value of angle α at that node. This is done in each iteration to find the

values of $\tilde{\mu}$ & k_g as well as at the end for parametric study.

(iii) The Roll Separating Force and Roll Torque:

The roll separating force and torque are determined after obtaining a converged solution as follows.

(a) Roll separating force:

The roll separating force per unit width of the plate is evaluated as the integral of the vertical traction component (t_y) over the arc of contact, expressed in terms of MN/m. Thus

$$\text{Roll separating force } F_y = \int_0^{l_g} t_y \, ds$$

where l_g is the total length of the arc of contact. However, in this analysis, this integral is evaluated numerically using 2 point gauss quadrature_

$$F_y = \sum_{i=1}^{2} \left((t_y)_i \, |J| \, w_i \right)$$

where t_y is the normal traction at the gauss point 'i', $|J|$ is the jacobian of the transformation from the boundary coordinates to the natural coordinates and w_i is the weight function.

(b) Roll torque:

The roll torque is evaluated by numerically integrating, by 2 point gauss quadrature , the elemental torque along the arc of contact as given below:

$$\text{Roll torque } T_r = \int_0^{l_s} R t_s \, ds = R \sum_{i=1}^{2} \left[(t_s)_i |J| w_i \right]$$

where " R " is the roll radius," t_s" is the tangential traction at the gauss point and $|J|$ and w_i are as defined above.

(iv) The Contours:

Contours are plotted to show the distribution of certain secondary parameters across the domain, namely for $\bar{\varepsilon}$, $\dot{\bar{\varepsilon}}$ and $\tilde{S}$. The contours for $\bar{\varepsilon}$ are plotted using the data at the nodes and for the later two, the plotting is done using the values evaluated at 2⊗2 gauss points of the elements from the converged solution.

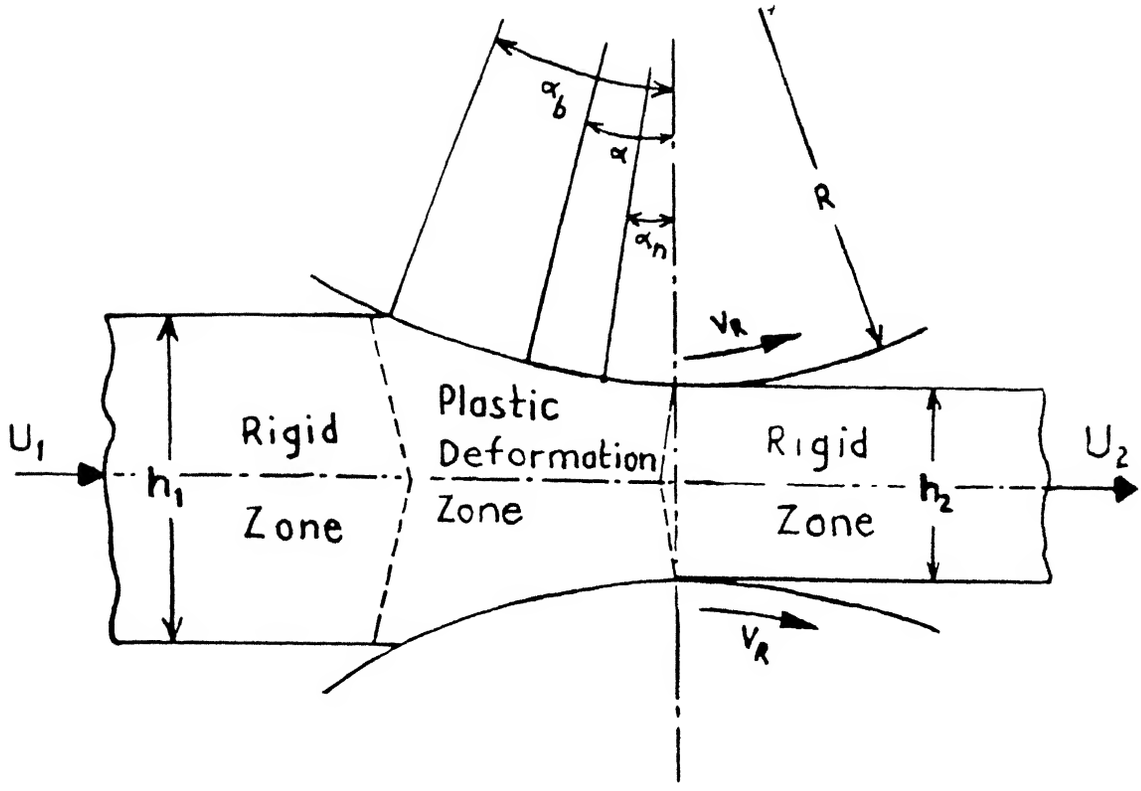

Fig. 2.1 The Flat Rolling Process

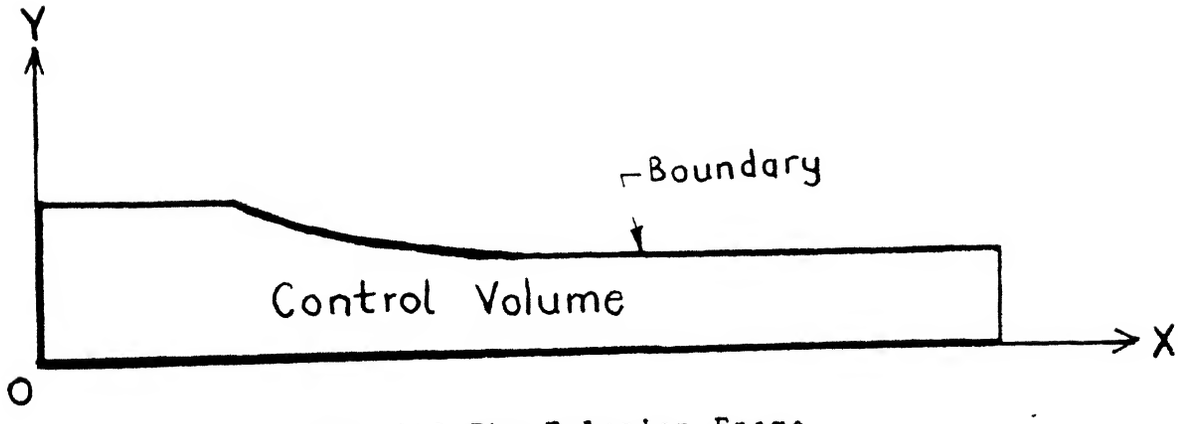

Fig. 2.2 The Eulerian Frame

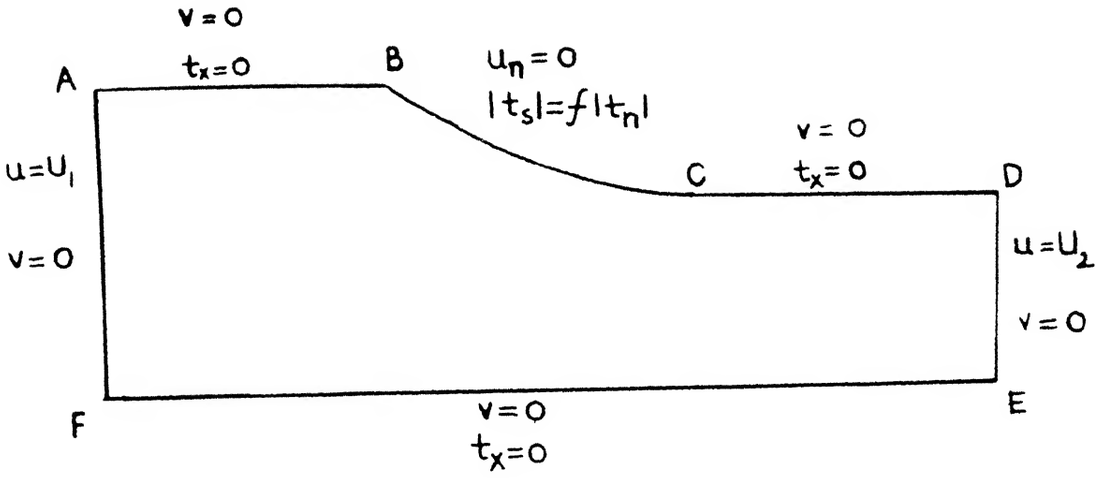

Fig. 2.3 The Boundary of the Domain and the Boundary Conditions

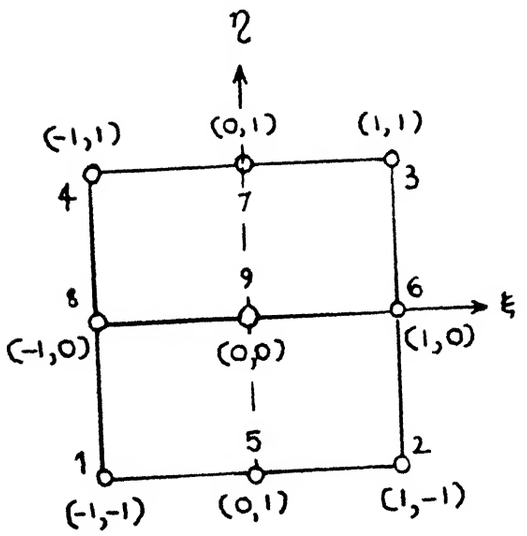

Element for
the interpolation of velocity

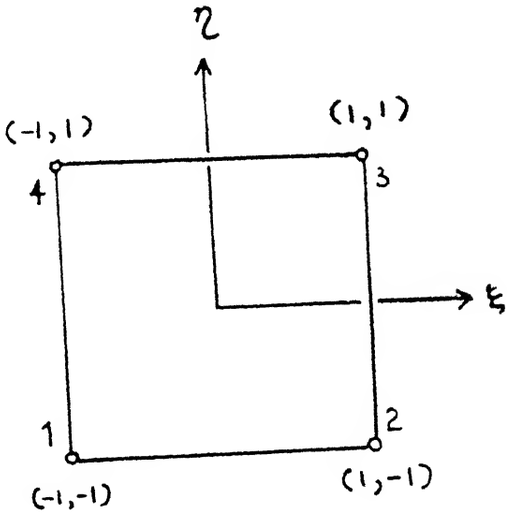

Element for
coordinate transformation

Fig. 2.4 A Typical Finite Element

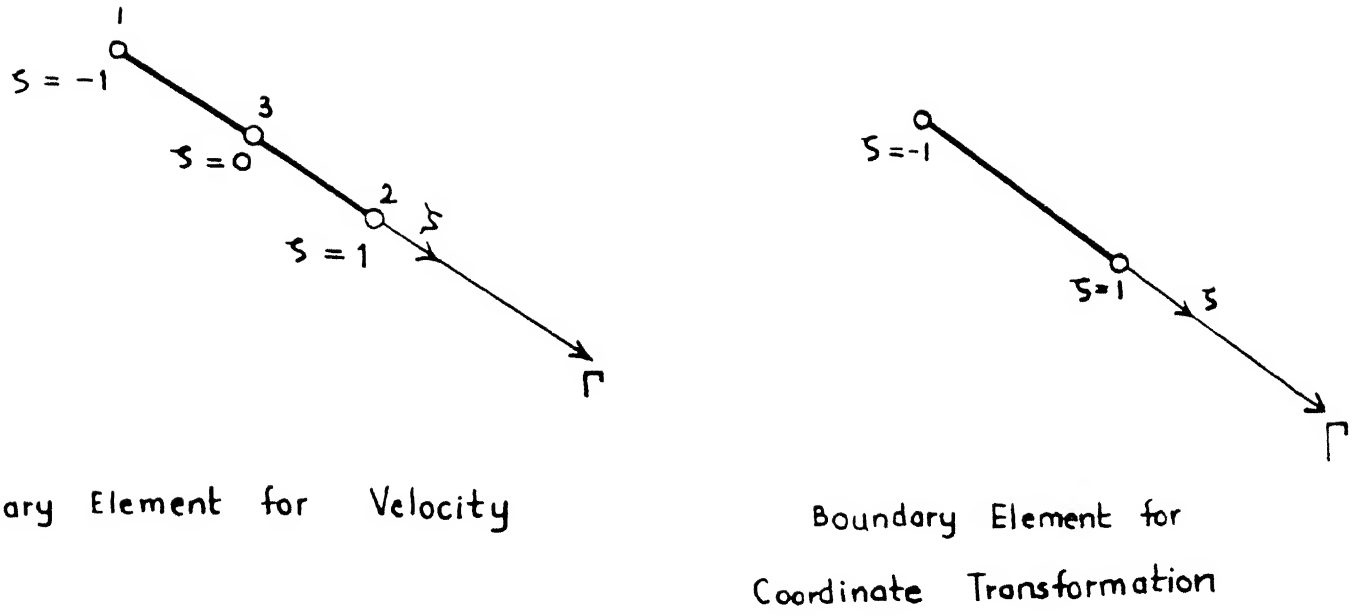

Fig. 2.5 A Typical Boundary Element

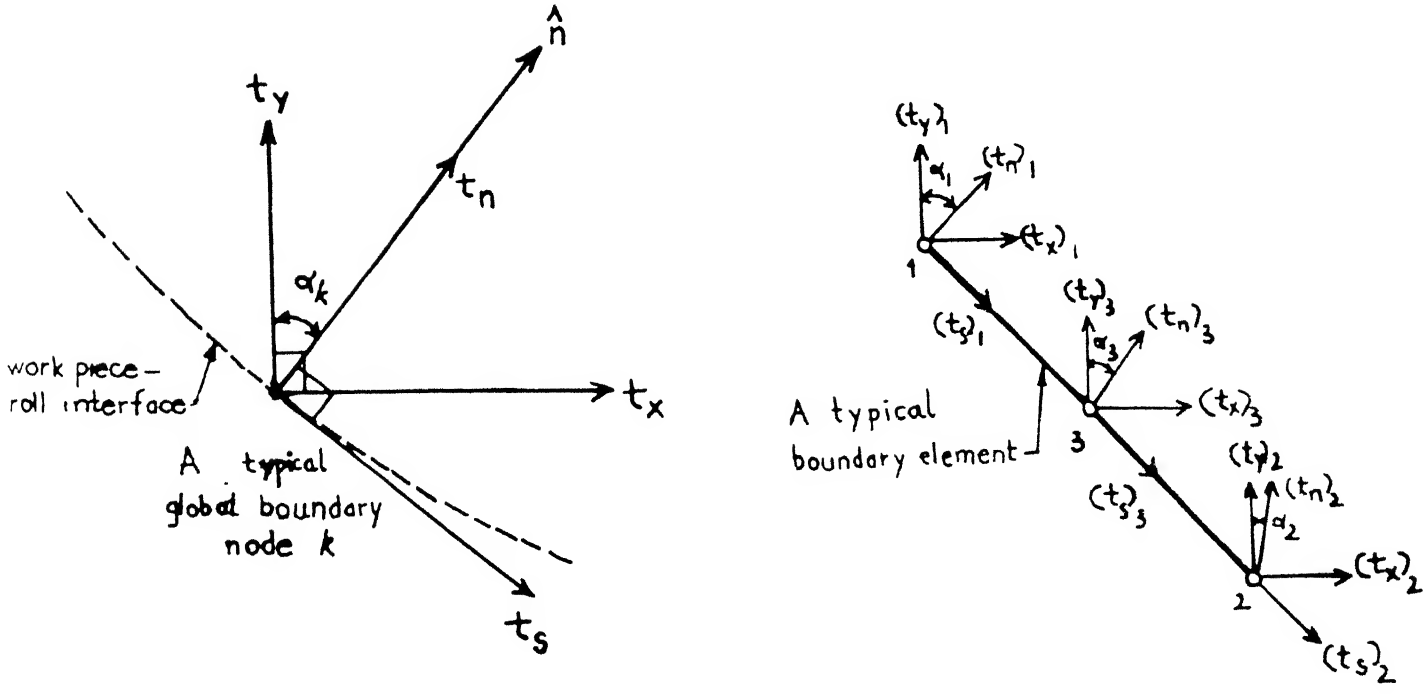

Fig. 2.6 The Boundary Tractions

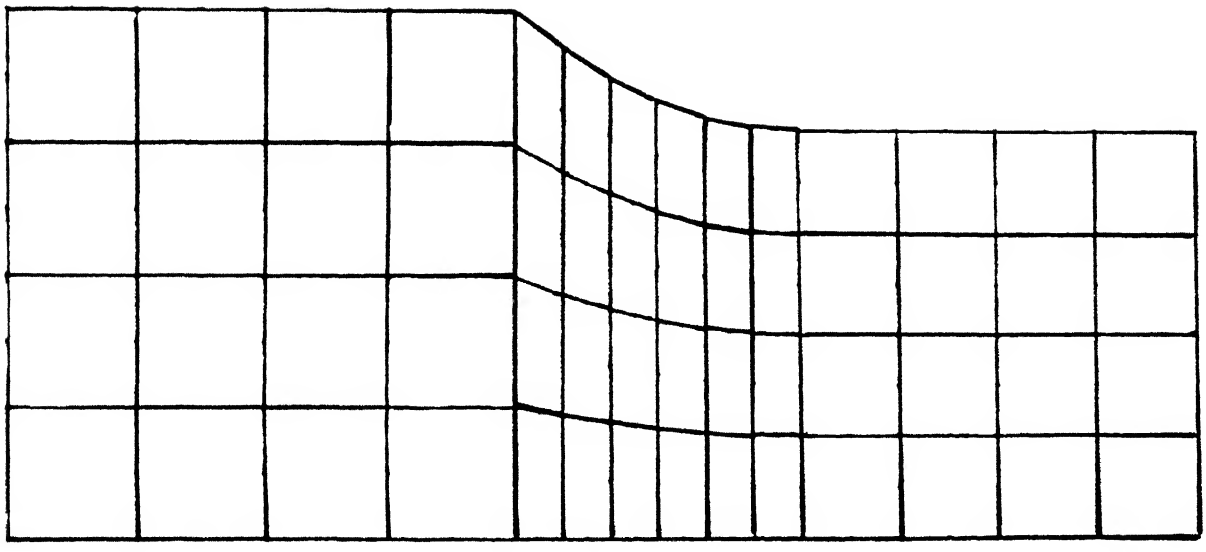

Fig. 2.7 The Finite Element Mesh

CHAPTER 3

RESULTS AND DISCUSSION

The finite element modelling of the physical problem of cold flat rolling developed in this work has been applied to a number of cases involving three metals and various non-dimensional input variables to illustrate its applicability.The metals considered are aluminium,mild steel and copper whose stress-strain relations are shown in table 3.1. The materials,dimensions and the strain-strain relations are considered in such a way that they are consistent with the cases considered in the works [12,15,25,26] so that the comparison is facilitated. In this work only comparisons with the experimental results are presented and rest of the emphasis is put on presenting a detailed parametric study and the effect of strain hardening. Comparison with the other analytical results is not given.Thus, in this chapter, the analytically obtained results are presented in four sections. In the first section the analytical results are compared with the experimental results of Al-Salehi et al [25] in case of aluminium and copper and Shida et al [26] in case of steel to validate the modelling and computations. In the second section, the parametric study, the effect of the three important rolling process variables viz. reduction ratio,the homogeneity factor (R/h1) and the coefficient of friction on the rolling parameters viz. normal pressure and shear stress distributions

along the arc of contact,roll separating force and roll torque are discussed. In the third section of this chapter, the error that can enter by ignoring the strain hardening effect is brought into light by comparing all the important design parameters without strain hardening and with strain hardening. The fourth section marks the end of the presentation of the results where a study of contours of normal strain-rates, equivalent strain rates,deviatoric stresses and equivalent strain is presented. In the penultimate section of this chapter conclusions are drawn as a post-analysis and evaluation of the work. In the last section suggestions for further research are included.

3.1. Validation

The validation of the results of the variation of the roll force (per unit width) with reduction ratio is presented in figures 3.1 to 3.6. The figures 3.7 to 3.12 show the comparison of the variation of the roll torque (per unit width) with reduction ratio. Finally the comparison of the distribution of pressure along the arc of contact is presented in figures 3.13 to 3.16.

It is clear from the figs.(3.1) to (3.6) that there is a good correlation between experimental and theoretical results of the roll force in case of steel and aluminium and to some extent that for copper. However, at higher reductions the deviation between them increases except for the case of R/h_1 =12.5 for aluminium.Similarly as can be seen in figures 3.7 to 3.12, in the case of roll torque, except for the case of aluminium with R/h_1=39, in all cases the deviation between analytical and

experimental results increases. While it is reported that the deviation is because of the assumption of constant coefficient of friction [15],it can also be attributed to the fact that at large values of reduction it becomes difficult to predict the neutral point accurately,which has a direct effect on the roll torque. Although the effect may not be at par with that of friction, the rigid roll assumption and the ignorance of entry and exit elastic effects are also expected to have contributed to the deviation of analytical and experimental results. Figures 3.13 to 3.16 show the comparison of analytical and experimental normal pressure distribution along the arc of contact. Although there is a considerable variation in magnitude, the important feature of multiple peaks of normal pressure at low values of R/h_1 and the friction-hill type of pressure distribution at higher values have been reproduced. The multiple peaks at low R/h_1 have been predicted also by the slip-line field solution of Firbank et al [8]. This suggests that the present model would be able to predict correct magnitudes of normal pressure over some range of values of R/h_1 reasonably accurately.

3.2. Parametric Study

In this section a discussion on the effect of process variables viz. reduction ratio,R/h_1 and the coefficient of friction on the normal pressure distribution,shear stress distribution,roll separating force and the roll torque is presented.

3.2.1. Effect of reduction ratio and R/h_1

The figure 3.17 depicts the variation of normal pressure(t_n)

along the arc of contact at different reductions. While the distribution is more uniform at higher reductions, at low reductions it is non-uniform and exhibits multiple peaks. It is interesting to note the peak point in the normal pressure curve at the entry which is the characteristic of all distributions.

The normal pressure, as shown in figure 3.18, increases rapidly with decreasing values of R/h_1 and becomes less smooth. Again the interesting observation is at low values of R/h_1 there is a distinct peak at the entry which is not to be seen at high values of R/h_1 , for example, R/h_1=130. However, at the exit the variation is smooth and uniform for all values of R/h_1.

Figure 3.19 shows the distribution of shear stress along the arc of contact from exit to the entry at different reductions. Since $|t_s|=f|t_n|$, at higher reductions t_s is more uniform similar to t_n. From figure 3.20, where the distribution of shear stress at different values of R/h_1 is shown, it is clear that the peak values of t_s also, similar to t_n, increase rapidly with decreasing R/h_1.

The variation of roll separating force with R/h_1 at different reductions is shown in figure 3.21. The figure suggests that while the roll separating force decreases with increasing R/h_1, at all reductions in the range, this decrease becomes more rapid at increasing reductions. This is consistent with the trend of t_n with R/h_1. This may be attributed to the indenting effect of roll into the work piece which increases with decreasing R/h_1. At a given R/h_1, roll separating force increases with reduction in spite of decrease in t_n. So the increase in contact area seems

to be having more effect than decreasing t_n on the roll separating force. Similar observations can be made in the figure 3.22 which shows the variation of roll torque with R/h_1 at different reductions. However, in the case of roll torque the decrease with R/h_1 at higher reductions is more monotonous. The continuous increase in roll torque with reduction at any given R/h_1 can be justified by referring to the variation of shear stress in figure 3.19, where it is clear that the percentage length of the backward slip zone (distance from the entry to the neutral point) at any given reduction increases with increasing reduction. Thus it follows that since the shear stress is positive in thebackward slip region roll torque increases with increasing reductions.

3.2.2. Effect of the coefficient of friction

The figure 3.23 shows the distribution of normal pressure along the arc of contact at different coefficients of friction. While the shape of the curve and smoothness are restored for all values of coefficient of friction, the peak magnitude increases with increasing coefficient of friction and peak seems to shift towards the entry. Figure 3.24 which gives the variation of shear stress along the arc of contact at different coefficients of friction. It can be noted from this figure that the peak magnitude increases with increasing coefficient of friction and that the neutral point shifts towards entry.

Figures 3.25 and 3.26 show the variation of roll separating force and roll torque with respect to the coefficient of friction, respectively. The modes of variation of roll force and

roll torque in these graphs can be appreciated by referring to the figures 3.23 and 3.24 where the normal pressure and shear stress distributions are depicted, respectively. It is interesting to see that since the contact area remains the same for all the three cases for which the curves are drawn, the variations, whatsoever, in roll force and roll torque are brought about by the change in shape and mode of variation of normal pressure and shear stress curves. From figure 3.25 it is evident that the roll force first increases with the coefficient of friction, however gradually, and then becomes uniform. This seems to be the consequence of the variation of normal pressure distributions which seem to become similar both in shape and magnitude with increasing coefficients of friction. Further the decreasing trend of roll torque curve with increasing coefficient of friction after reaching a peak can be appreciated by observing the figure 3.24. Here it is very clear to observe that with increasing coefficient of friction not only the neutral point shifts towards the middle of the arc of contact but the difference between negative and positive average values of shear stress decreases, both leading to a net decrease in the roll torque with increasing coefficient of friction. However, meanwhile the fact that the computer program in this analysis ceases to converge for the values of coefficient of friction beyond 0.29 should also be pointed out.

3.3. Effect of Strain Hardening

In this section the effect of strain hardening is brought into light by selecting two sets of process variables. In the

first set the process variables are such that they are expected to give a minimum value of the design parameter to be obser ed and in the second set they give an expected maximum of the same. These expectations are based on the foregoing parametric study. The design parameters are the same which were considered for parametric study. While the discussion for the former two is given by means of graphs, the later two are presented in the table 3.2. The percentage deviation for peak magnitudes of normal pressure and shear stress are also included in the table 3.2.

The figure 3.27 contains the distribution of normal pressure without and with strain hardening for the two sets of process variables. While it is clear to see that the normal pressure is higher with strain hardening than without strain hardening all along the arc of contact in both the sets, the peak deviation occurs near exit in the first set whereas it occurs in the middle of the arc of contact in the second set. Further the percentage error in the estimation of t_n when the strain hardening effect is neglected is more for the set 2 (see the table 3.2). It can be noted that the variation of t_n along the arc of contact is more uniform for the set 1 than for set 2. Figure 3.28 shows the effect of strain hardening on the shear stress distribution along the arc of contact for the same two sets of process variables. It shows that the percentage deviation is more for set 2. The underestimation of roll force and roll torque by not considering the effect of strain hardening is presented in table 3.2.

3.4. The Study of Contours

The figures 3.29 to 3.32 show the contours for the normal-strain rate, equivalent strain-rate, deviatoric stress invariant and the equivalent strain in the domain for four sets of values of the three process variables. The four sets are so selected that the comparison with the contours of the first set of any of the successive three sets gives the effect of one process variable on the distribution of that parameter in the domain. The graphics routine for plotting these contours has been developed along with the computer program for the main finite element analysis.

The figure 3.29 shows the contours for normal strain rate for steel for the four sets of process variables in (a),(b),(c) and (d). The normal strain rates, at any given set of process variables first increase from a small value as the metal enters the deformation zone and reach a maximum and thereafter decrease gradually as the metal exits from the deformation zone. However, a marked difference can be observed between these trends along the surface where the work piece is in contact with the roll and along the axis of symmetry. While the normal strain rates along the axis of symmetry uniformly increase, reach a maximum and then decrease to a small value, just as explained above as a typical nature, along the work piece-roll interface they undergo a non-uniform variation with multiple maximums and minimums from inlet to the exit. This variation from uniform along the axis of symmetry to non-uniform along the interface is gradual. Because of this inhomogeinity of deformation pockets of normal strain

rates result along and just below the interface. It can be observed from the figure 3.29 (a), (b), (c) and (d) that with increased reduction ratio (a to b) the homogeinity of deformation increases and with increased R/h_1 and coefficient of friction the inhomogeinity increases (a to c and a to d, respectively). The normal strain rates in 3.29(a) first increase and reach a maximum value at the first contact point. Then it decreases towards the middle of the arc of contact reaching a minimum. It then again increases and attains another peak value and continuously decreases towards exit. They have two peaks on the surface and a minimum. With increased reduction, as shown in 3.29(b), the number of peaks reduce to one which occurs at a point away from the first contact point. Further the normal strain rates continuously increase till the peak is reached and then continuously decrease till they reach the cut off value at the exit. The increasing coefficient of friction and decreasing R/h_1 seem to have little effect on the distribution of normal strain rates, as can be seen from 3.29(c) and 3.29(d). However, a minimum is introduced before a contour goes down to cut off value at the exit. Similar observations are possible from the equivalent strain rate contours shown in the figure 3.30.

The contours of deviatoric stress invariant which is a measure of stress at any point required to cause a given amount of plastic strain at that point . In general, at any given set of process variables, the equivalent deviatoric stress first rapidly increases at the entry as the loading occurs, continues to increase into the deformation zone reaching a maximum somewhere

in the middle and then gradually decreases towards exit. However, at the exit where unloading of the work piece occurs , the decrease in the deviatoric stress invariant is again very rapid as the metal comes out of the deformation zone. Although the effective deviatoric stress remains more or less uniform across the rolling direction in the work piece at the loading and unloading points the variation between and surface particles is distinct. This observation is common to all sets in the figure 3.31 except that the variations at the inlet and exit are not shown in any of these figures. Comparison of figure 3.31(b) with figure 3.31(a) suggests that the deviatoric stresses become more or less uniform across the section with increased reductions. However, there is not much effect of other two process variables on the distribution of these contours. The figure 3.32 shows the contours of equivalent strain, also in four sets.The following observations can be made from the figures for the contours of equivalent strain. At the entry as the metal enters into to the deformation zone the strain increases rapidly from a very low value. In this zone clearly the surface particles undergo higher amounts of strain than those inside. As the metal progresses towards the exit, however, the inside particles catch up and trend becomes almost reverse. While the trend at higher reduction ratios is more or less similar, because of longer path available for the particles to travel from the inlet to the exit this variation is gradual. Equivalent strains at higher coefficient of friction are shown in figure 3.32(a) keeping the other variables constant. This illustrates that at higher friction the surface

particles are too highly strained to be reached by the inside particles and therefore throughout the domain the equivalent strain across the sections increases from inside to the surface. This variation is gradual from a low value to a high value.

3.5. Conclusions

Based on the above discussions the following conclusions can be drawn. In the present analysis cold plane-strain flat rolling problem is solved by the finite element method at steady state by considering the material to be rigid-plastic strain hardening. The model can give good results over a range of the process variables viz. the reduction ratio, R/h_1 and the average coefficient of friction. The model has the capability of accommodating variable coefficient of friction which can be considered from the experimental results to obtain better results. In this work a detailed parametric study has been conducted to manifest the effect of the process variables on the important design parameters of rolling process. The error of the assumption of perfectly plastic material is highlighted. Contours have been shown to illustrate the distribution of stresses, strain rates and strains for an understanding of the physical process of rolling.

3.7. Scope for Further Research

As has been indicated in the above lines, the model is certainly amenable to the inclusion of the variable coefficient of friction which can further improve the accuracy of results. It should also be pointed out that, a change in the mesh by bringing in smaller elements at appropriate places is likely to improve

the results. While three dimensional treatment is not an improvement over every 2-D analysis(especially when the width/thickness is very high the cost incurred in 3-D analysis can prove to be too high to appreciate the extra accuracy achieved), by carrying 3-D analysis some additional features like profile of the strip can be brought into light and the problems of shape rolling where the flow of metal in the third direction is significant to achieve the required shapes can be dealt with. The assumption that the metal is rigid at the entry and exit and that the roll is rigid may also be eliminated to predict better results.

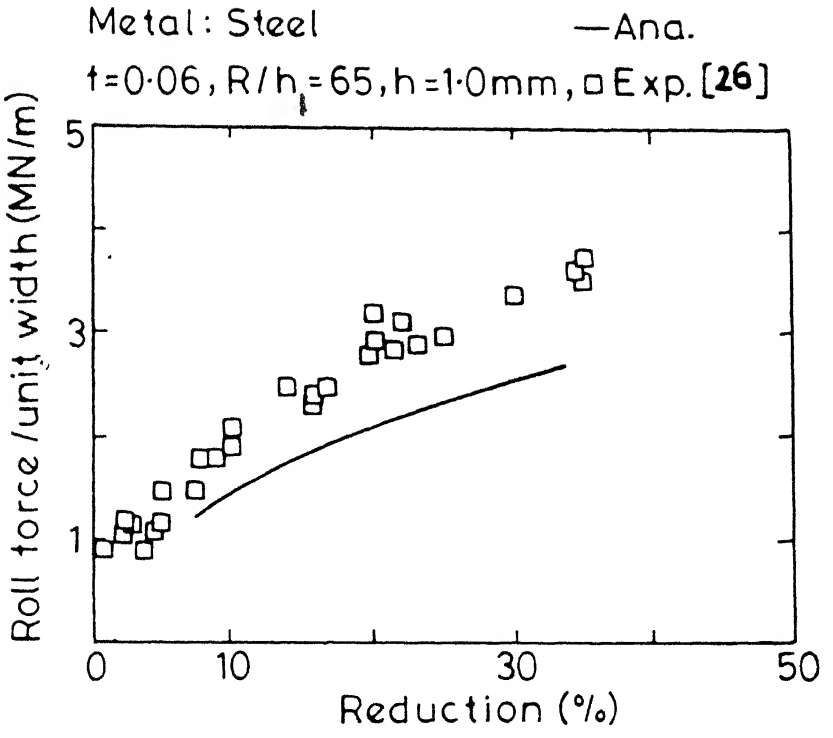

Fig. 3·1 Comparison of Analytical and Experimental Roll Force

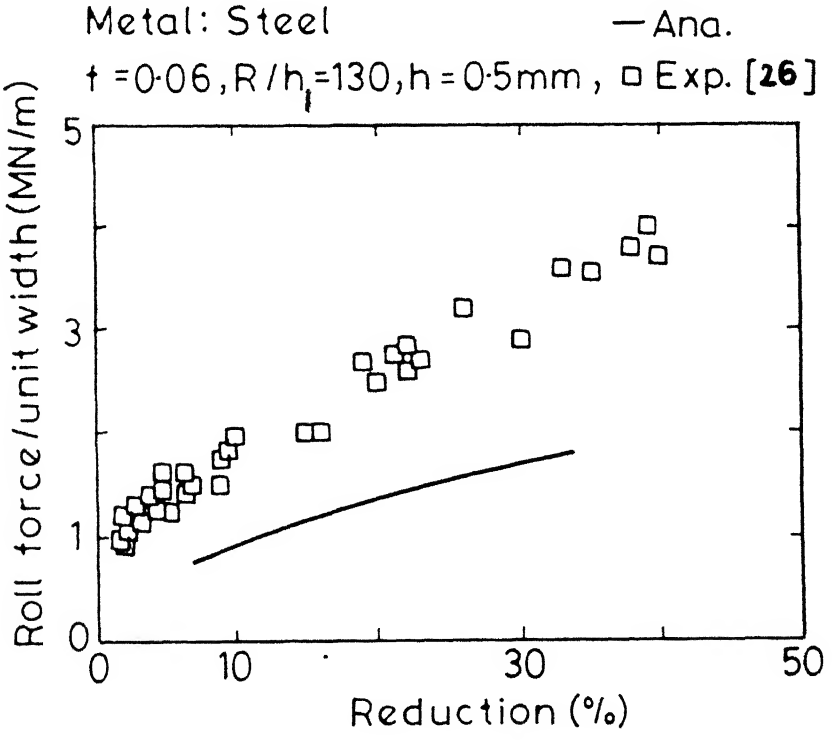

Fig. 3·2 Comparison of Analytical and Experimental Roll Force

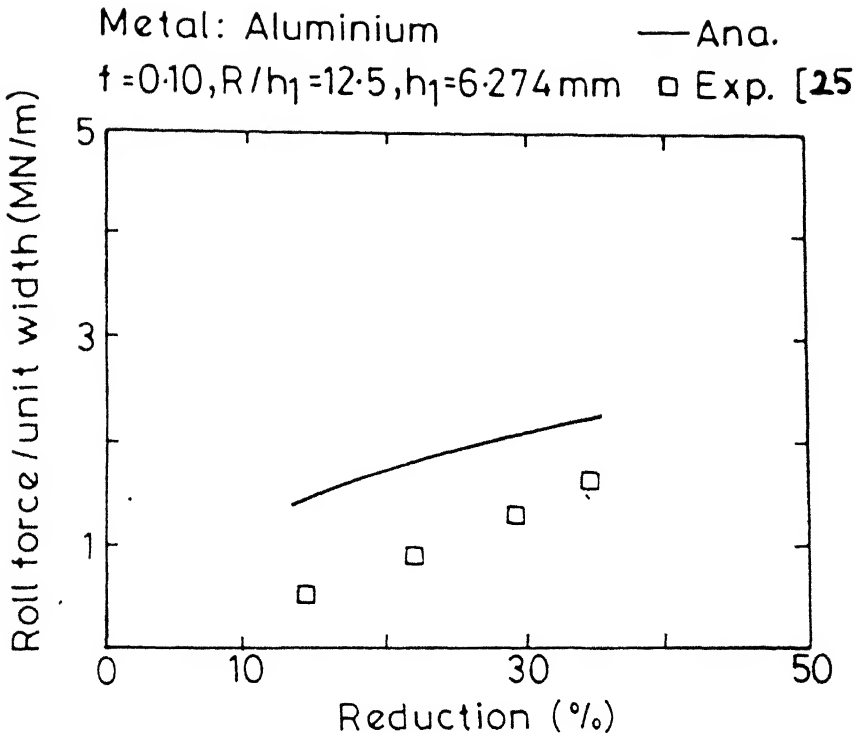

Fig. 3·3 Comparison of Analytical and Experimental Roll Force

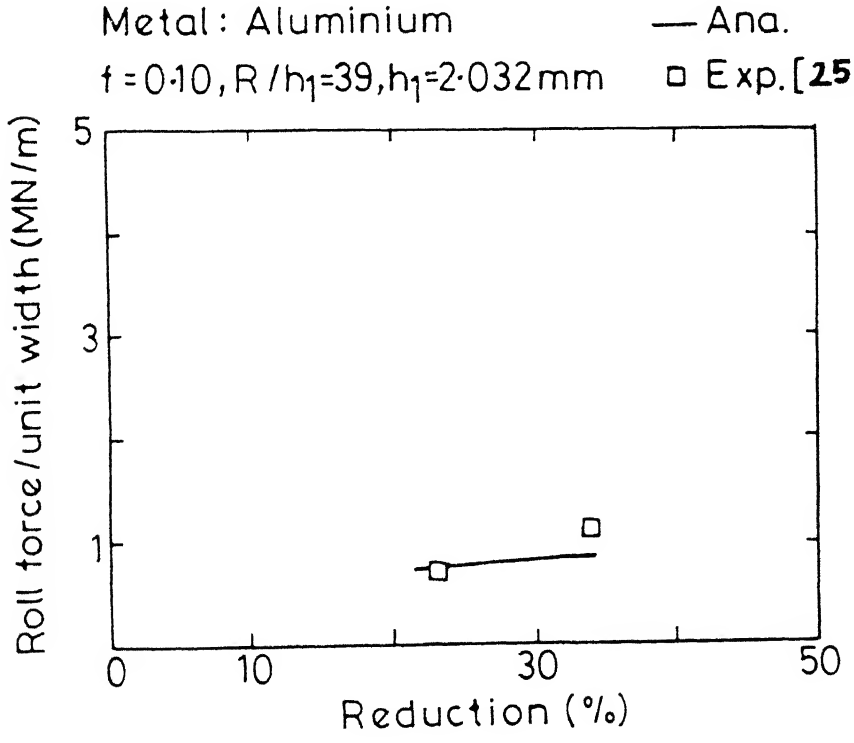

Fig.3·4 Comparison of Analytical and Experimental Roll Force

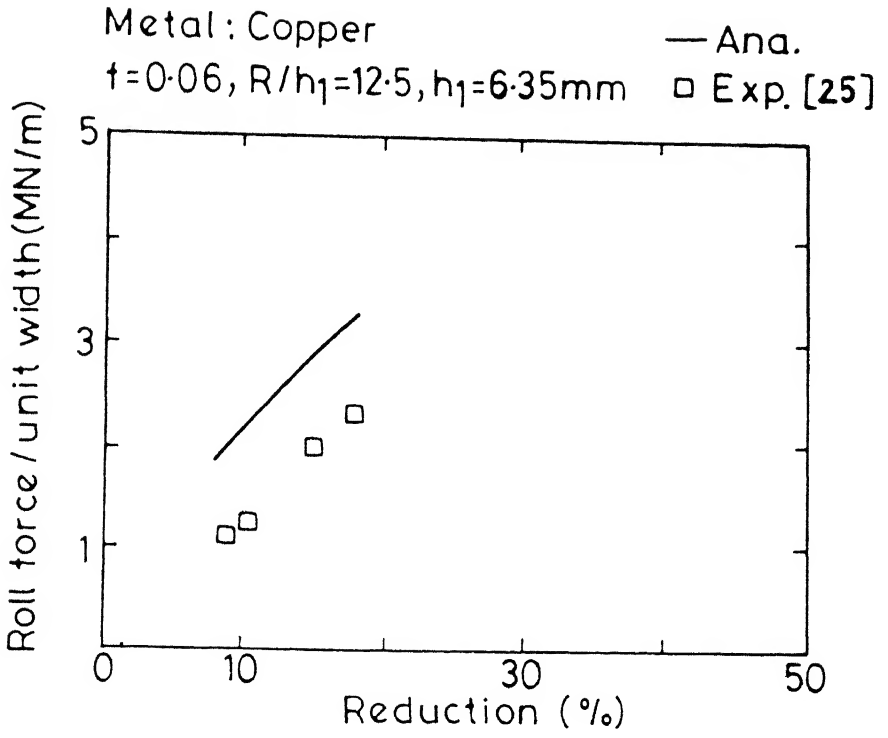

Fig.3·5 Comparison of Analytical and Experimental Roll Force

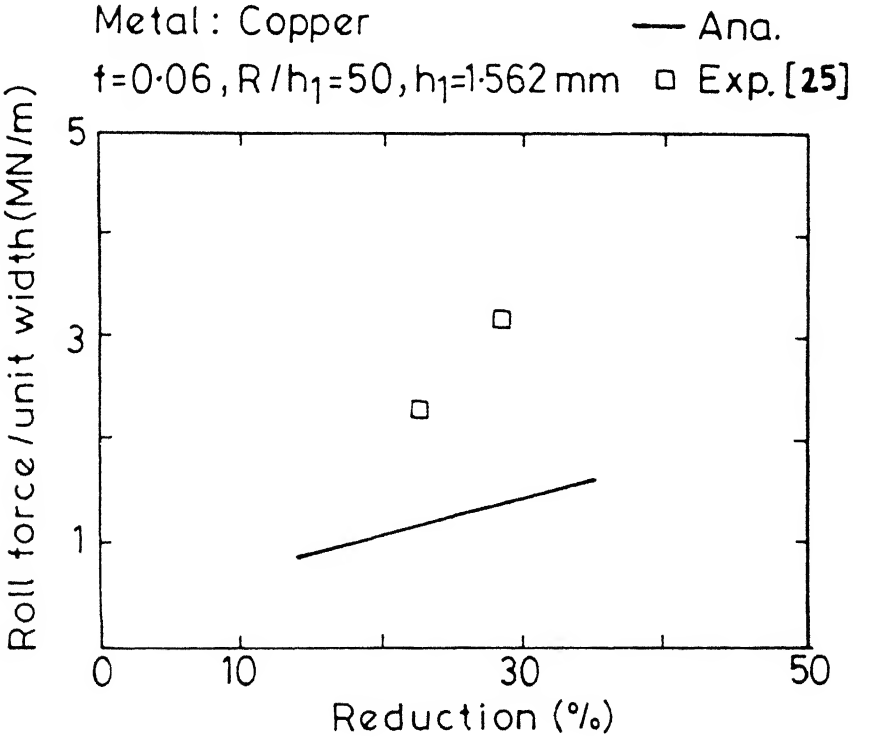

Fig.3·6 Comparison of Analytical and Experimental Roll Force

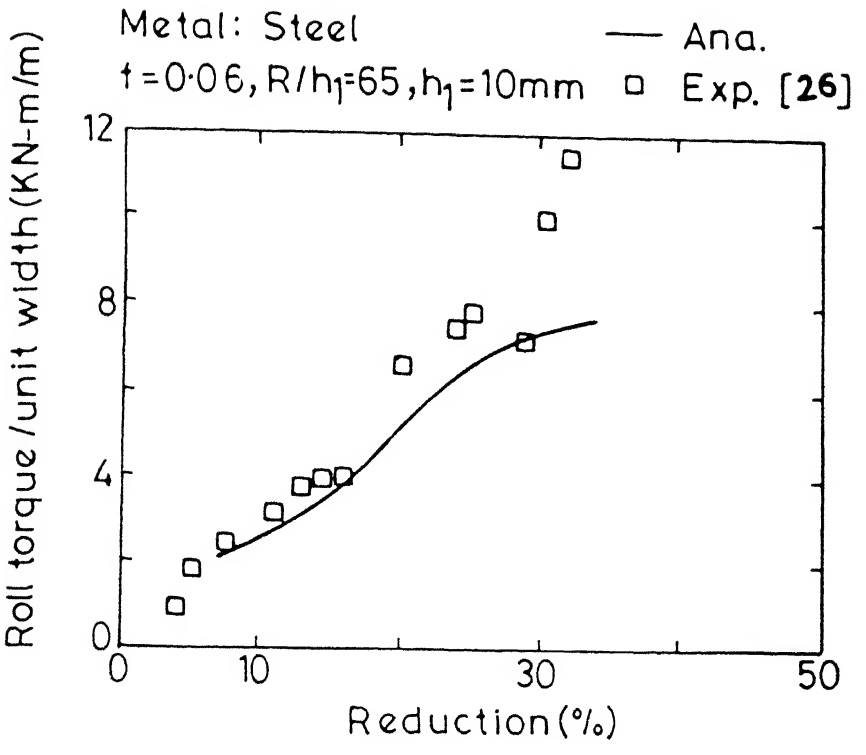

Fig.3·7 Comparison of Analytical and Experimental Roll Torque

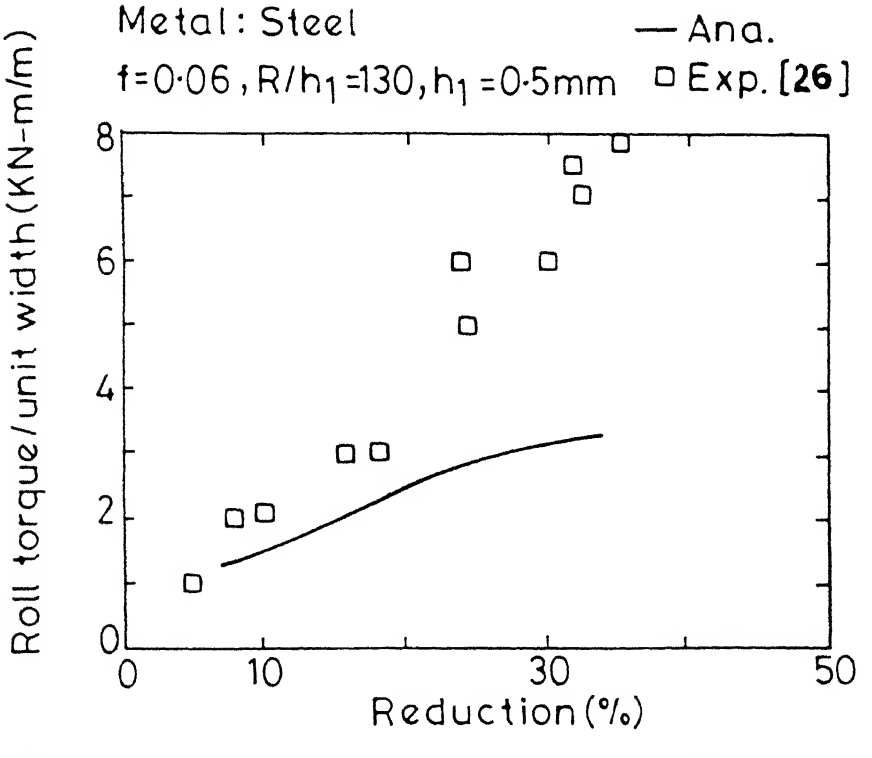

Fig.3·8 Comparison of Analytical and Experimental Roll Torque

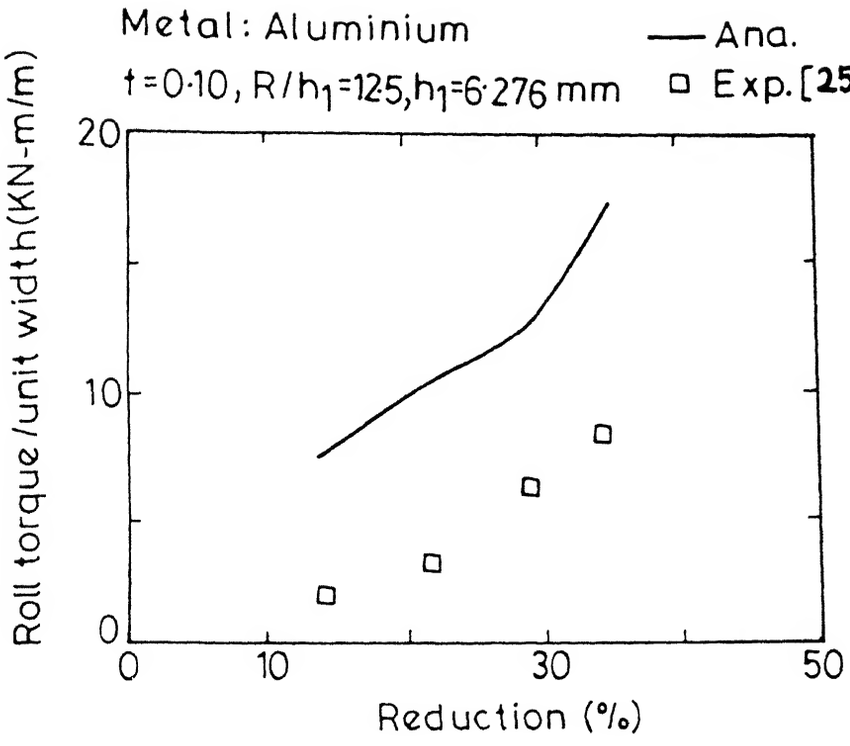

Fig.3·9 Comparison of Analytical and Experimental Roll Torque

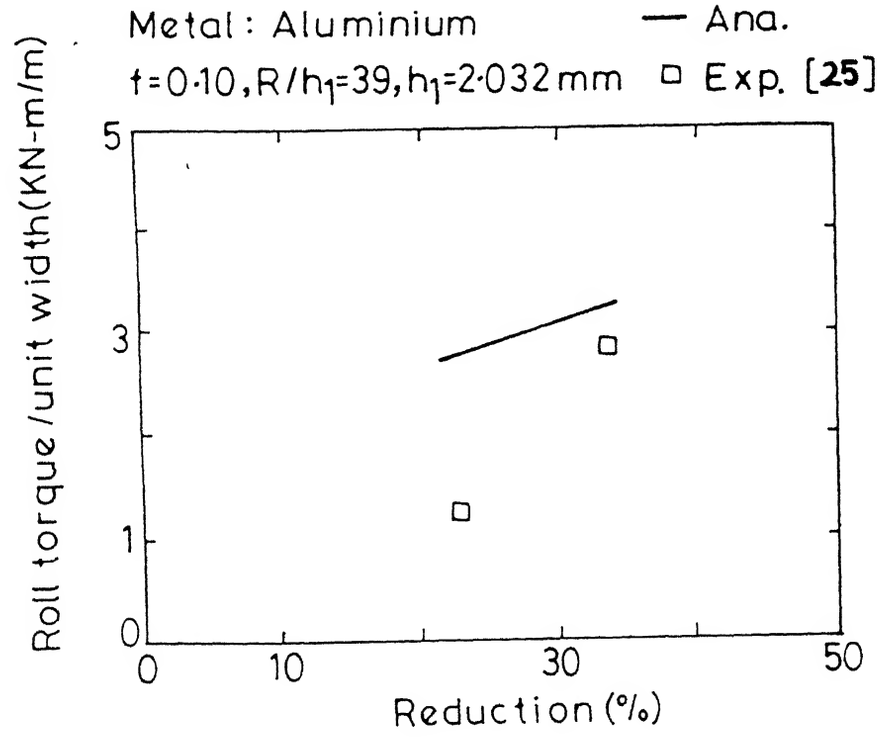

Fig.3·10 Comparison of Analytical and Experimental Roll Torque

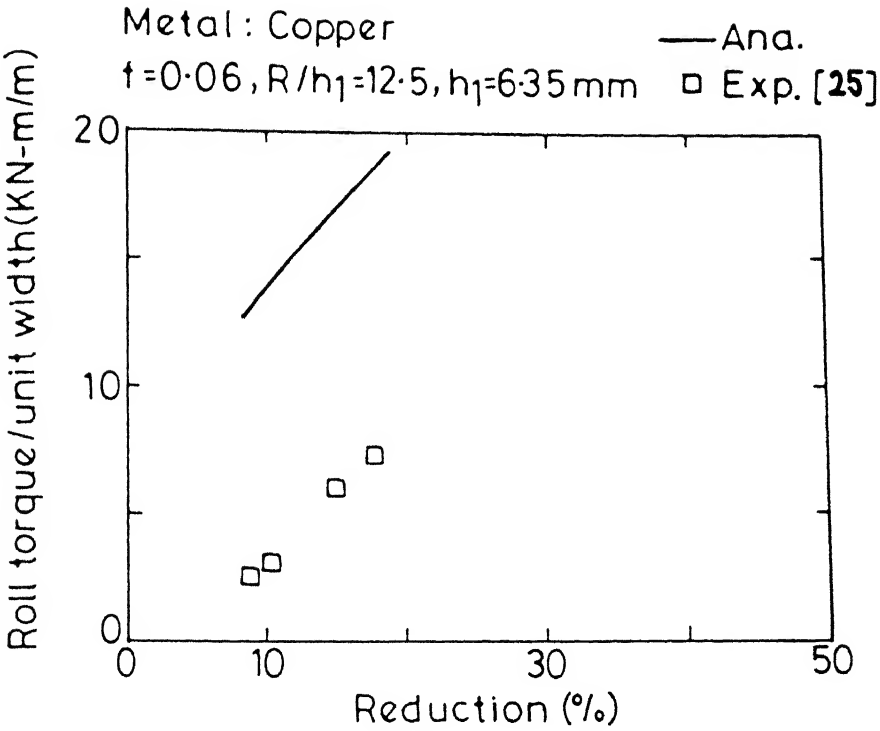

Fig.3·11 Comparison of Analytical and Experimental Roll Torque

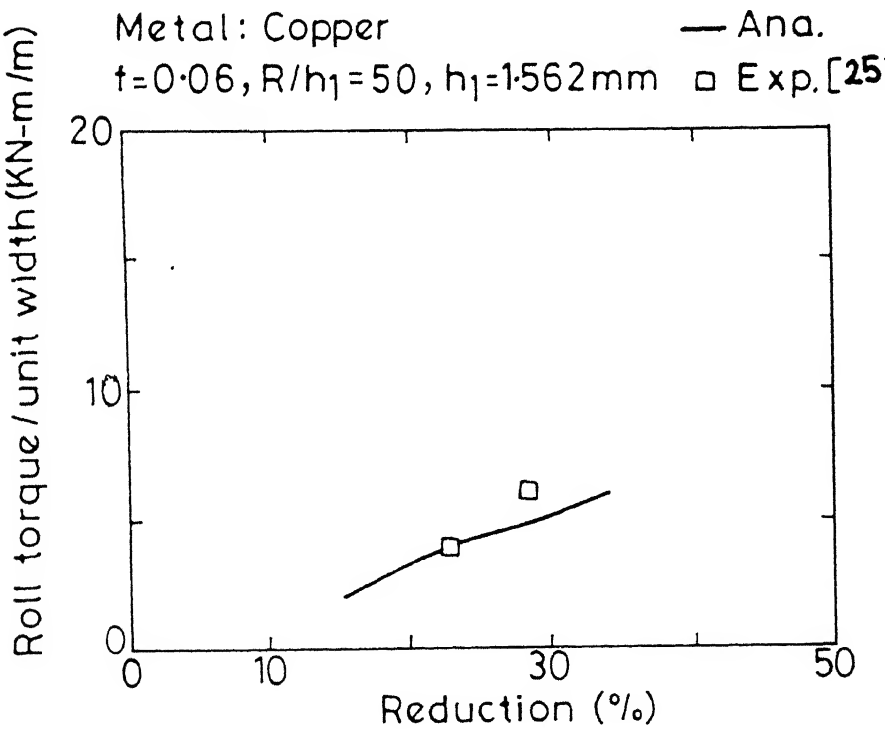

Fig.3·12 Comparison of Analytical and Experimental Roll Torque

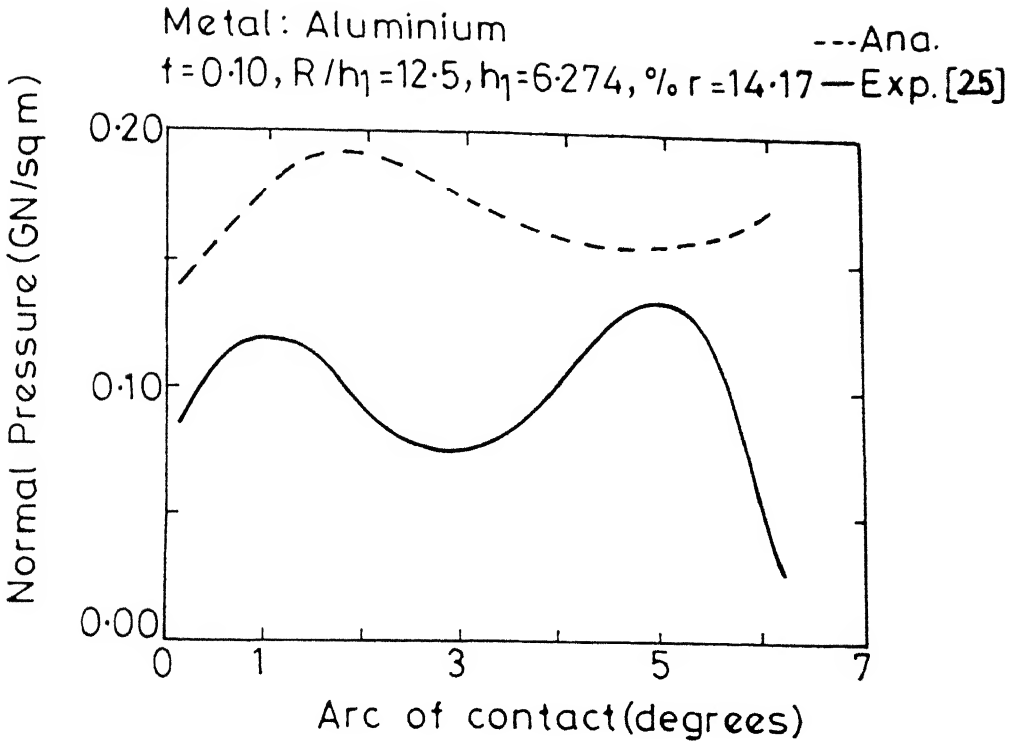

Fig. 3·13 Comparison of Analytical and Experimental Normal Pressure

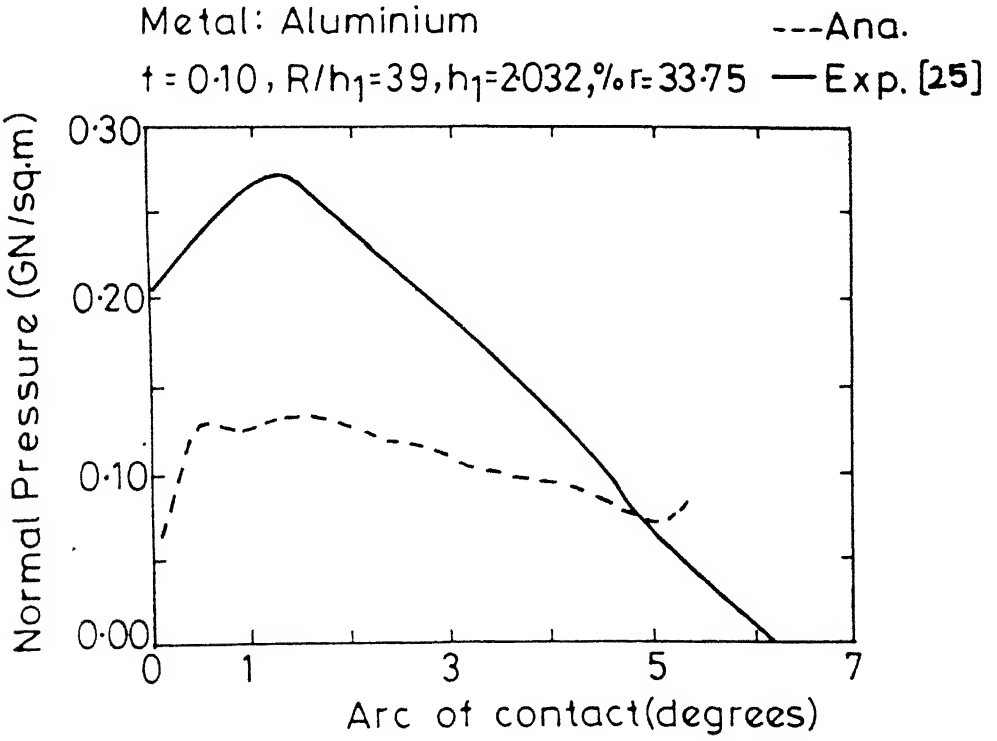

Fig. 3·14 Comparison of Analytical and Experimental Normal Pressure

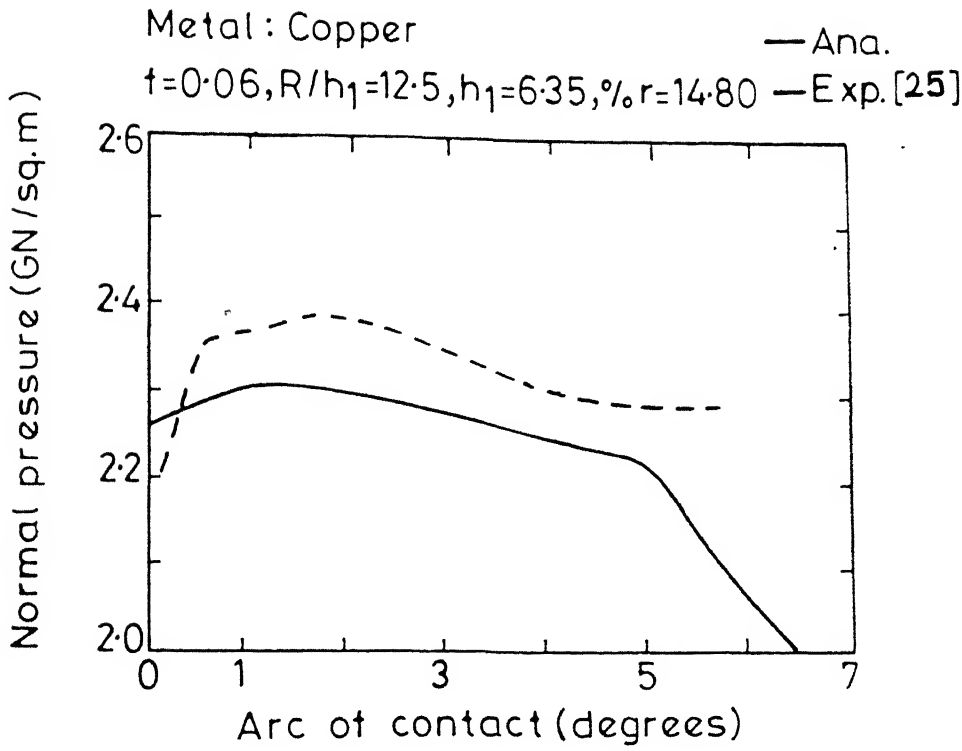

Fig.3·15 Comparison of Analytical and Experimental Normal Pressure

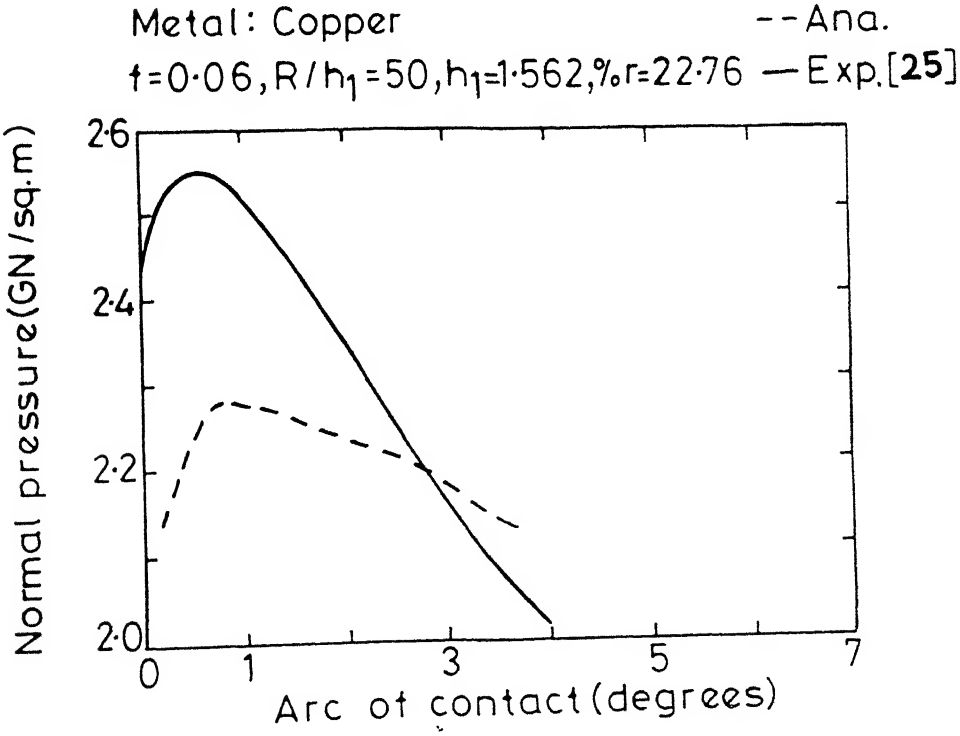

Fig.3·16 Comparison of Analytical and Experimental Normal Pressure

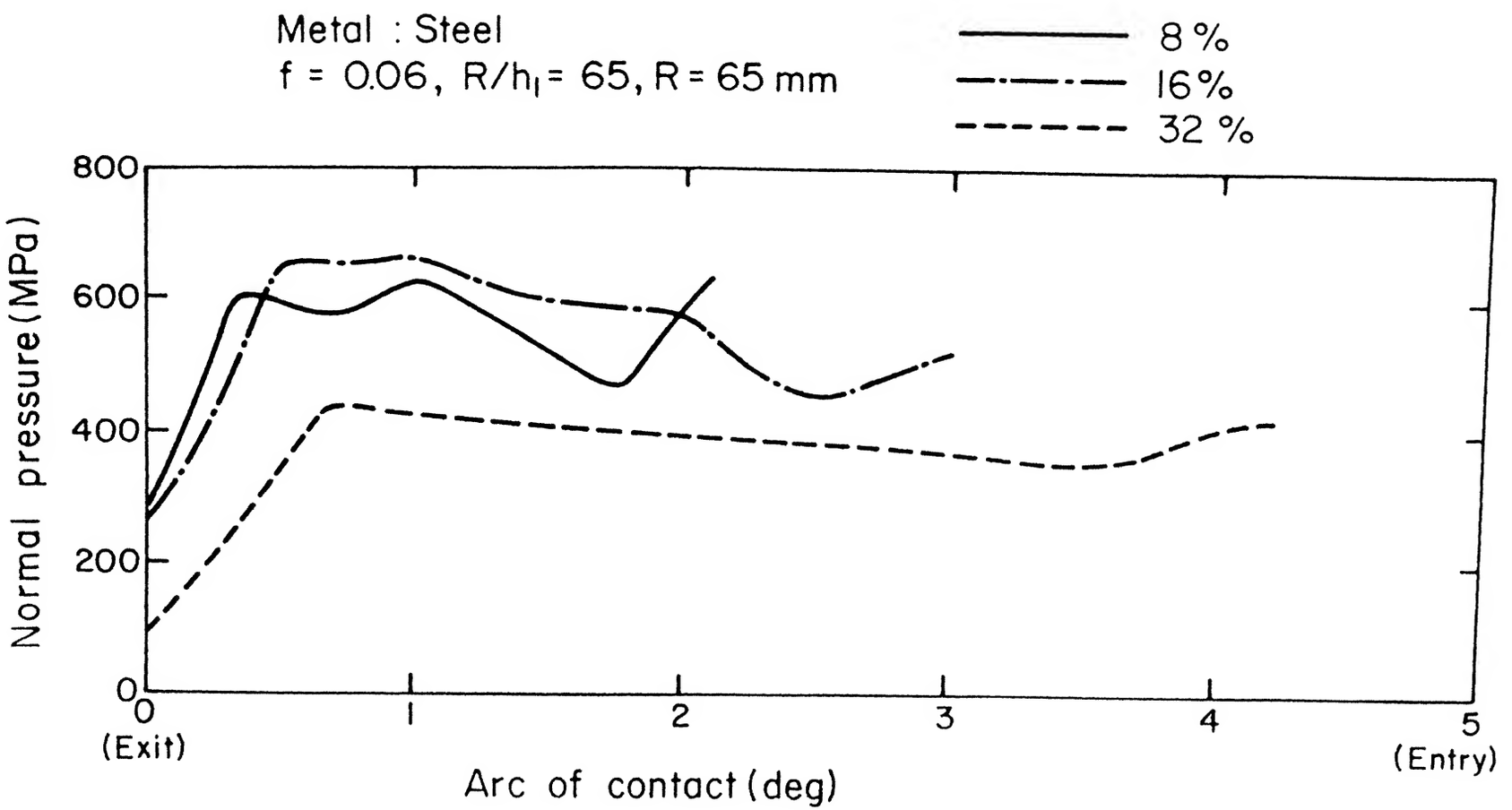

Fig.3.7 Distribution of normal pressure at different reductions

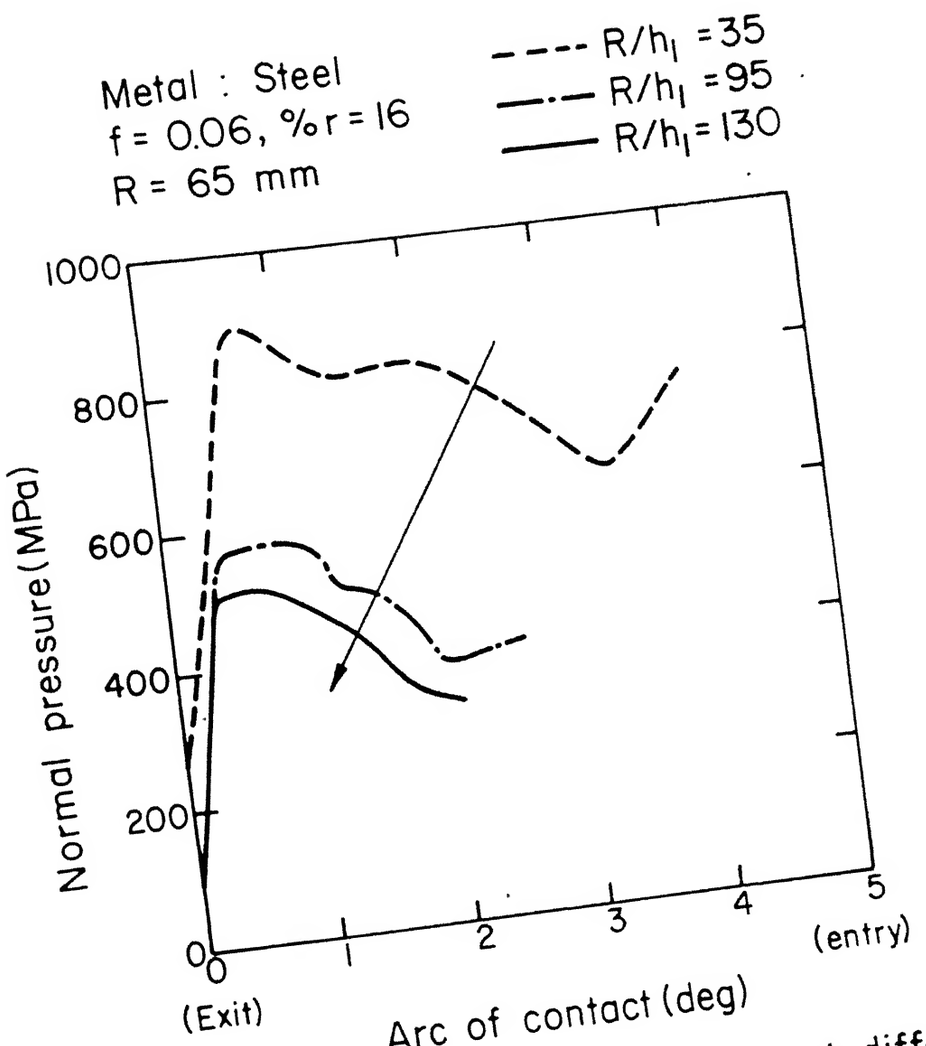

Fig.3.18 Distribution of normal pressure at different values of R/h_1

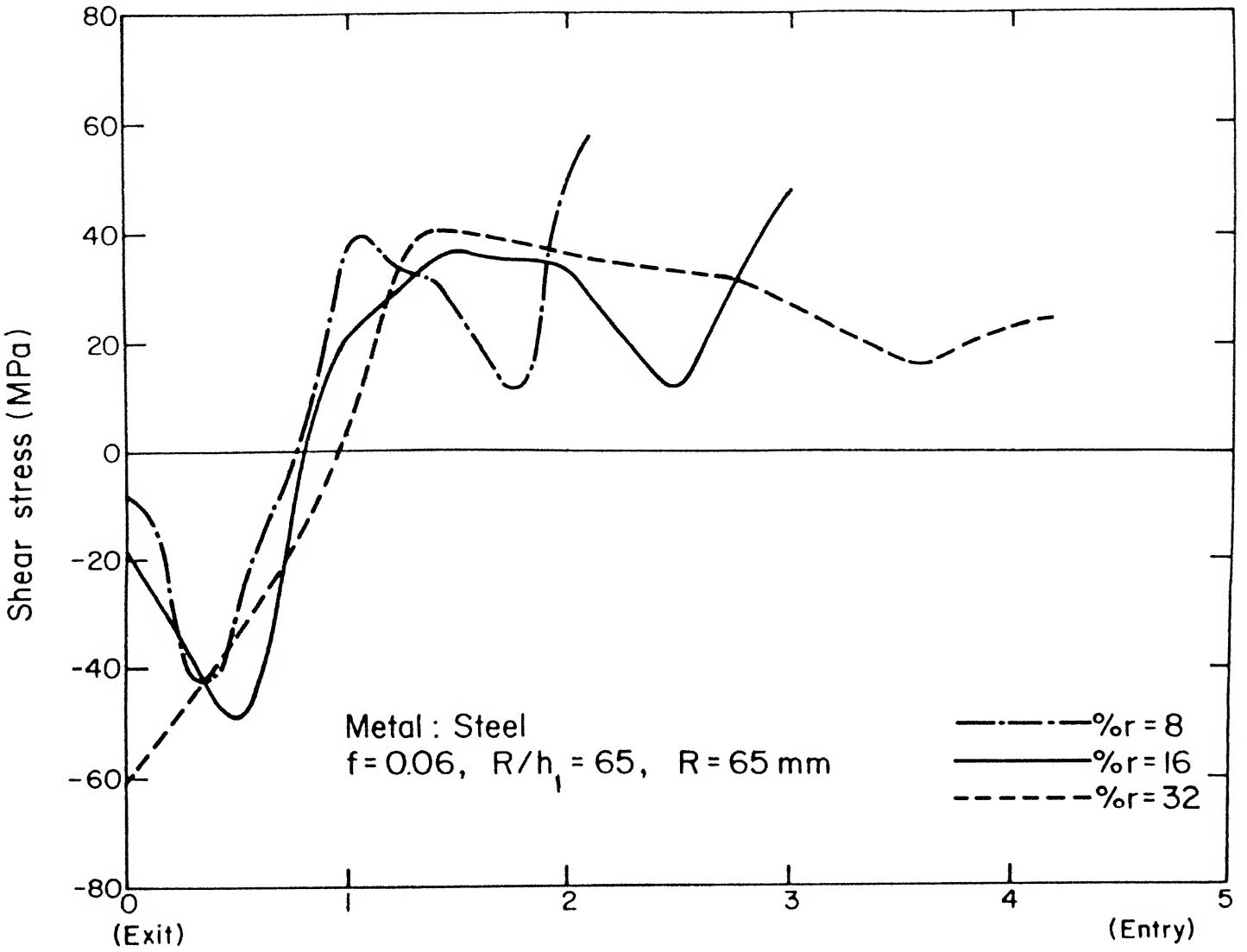

Fig.3.19 Distribution of shear stress at different reductions.

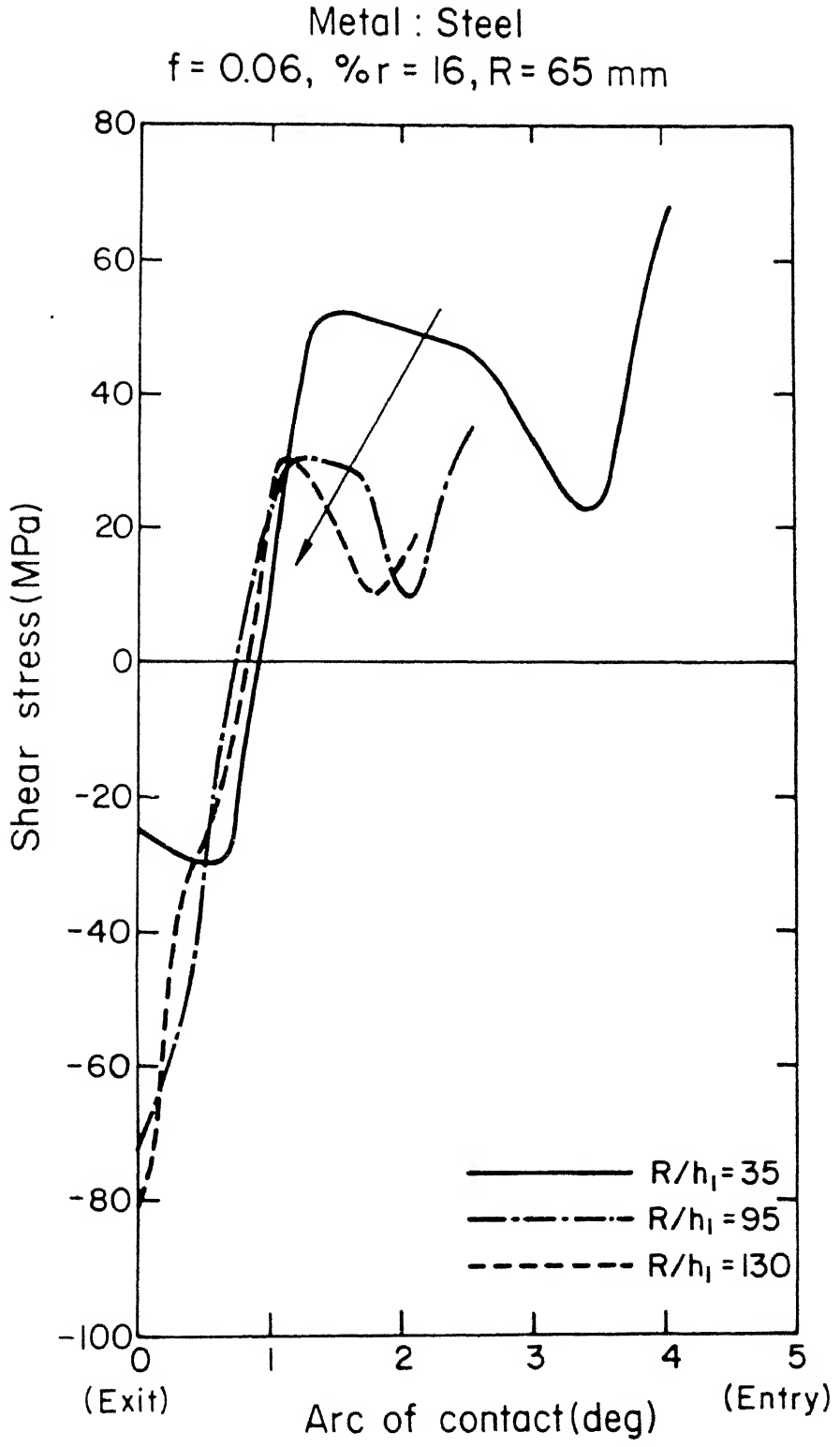

Fig.3.20 Distribution of shear stress at different values of R/h_1.

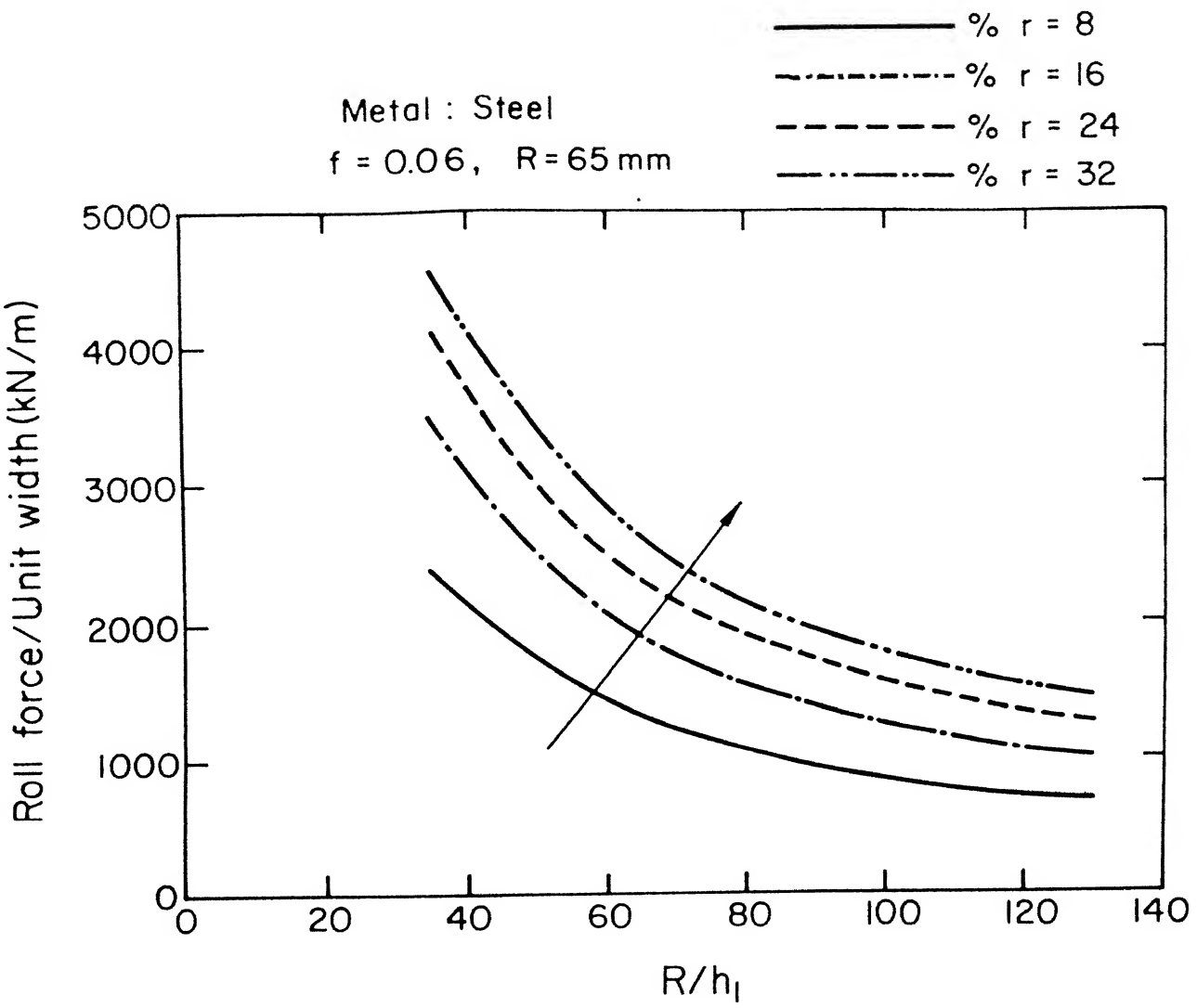

Fig.3.21 Variation of roll separating force with R/h_1 at different reductions.

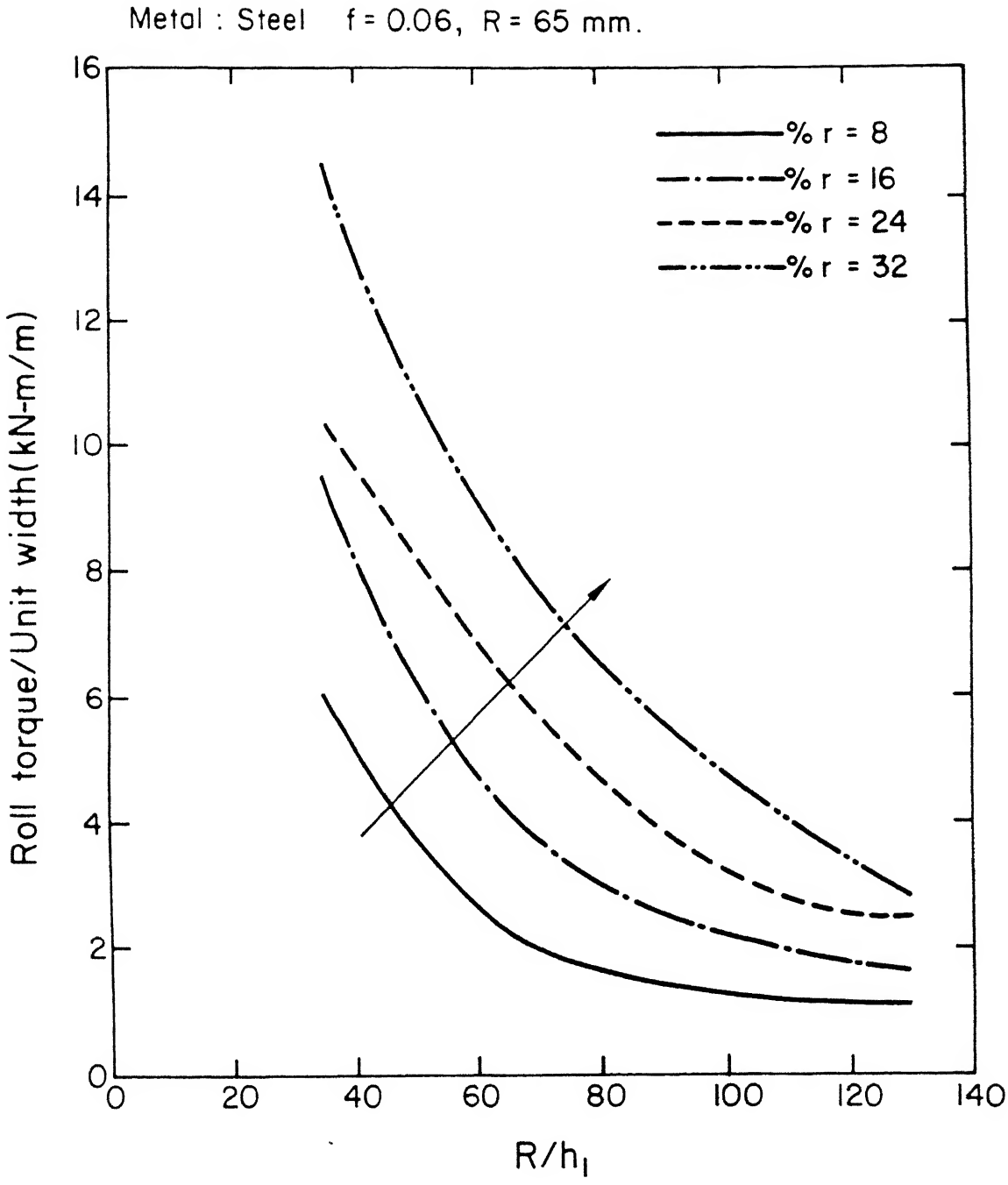

Fig.3.22 Comparision of variation of roll torque with R/h_1 at different reductions.

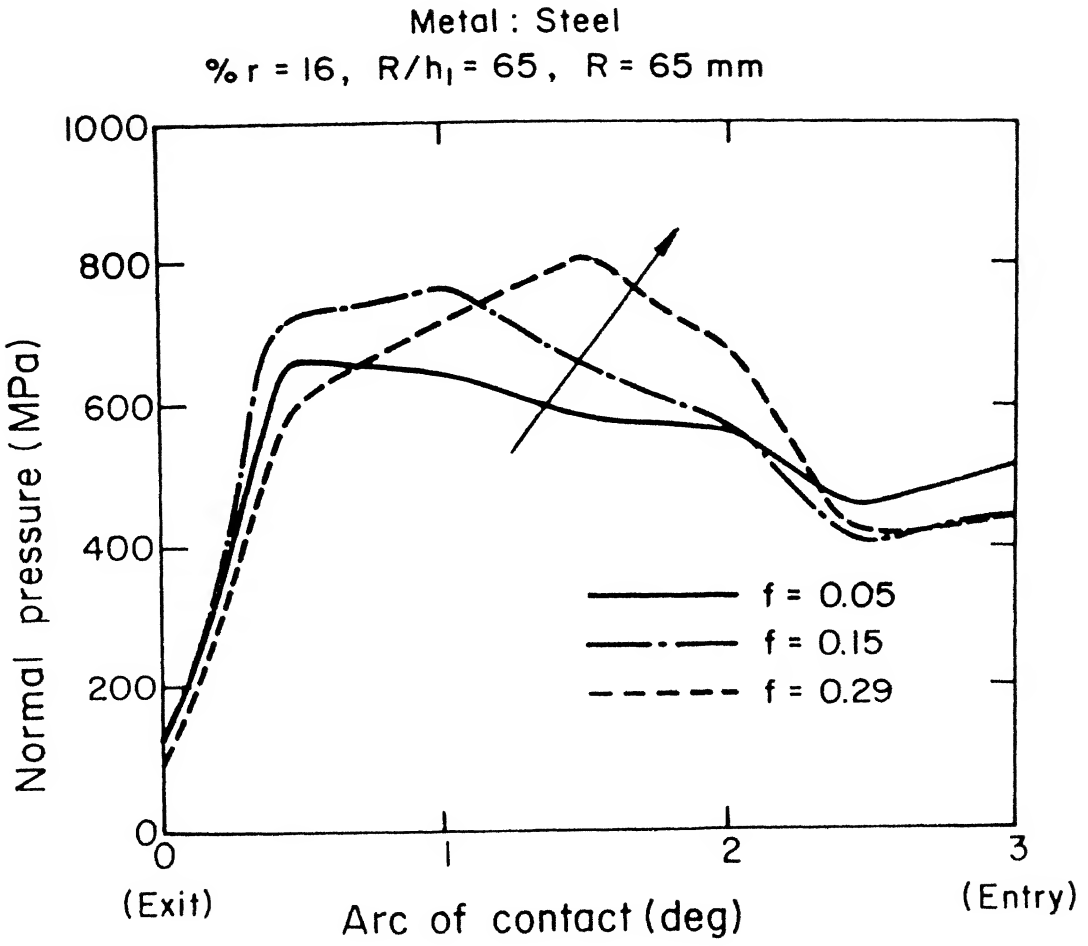

Fig.3.23 Distribution of normal pressure at different coefficients of friction.

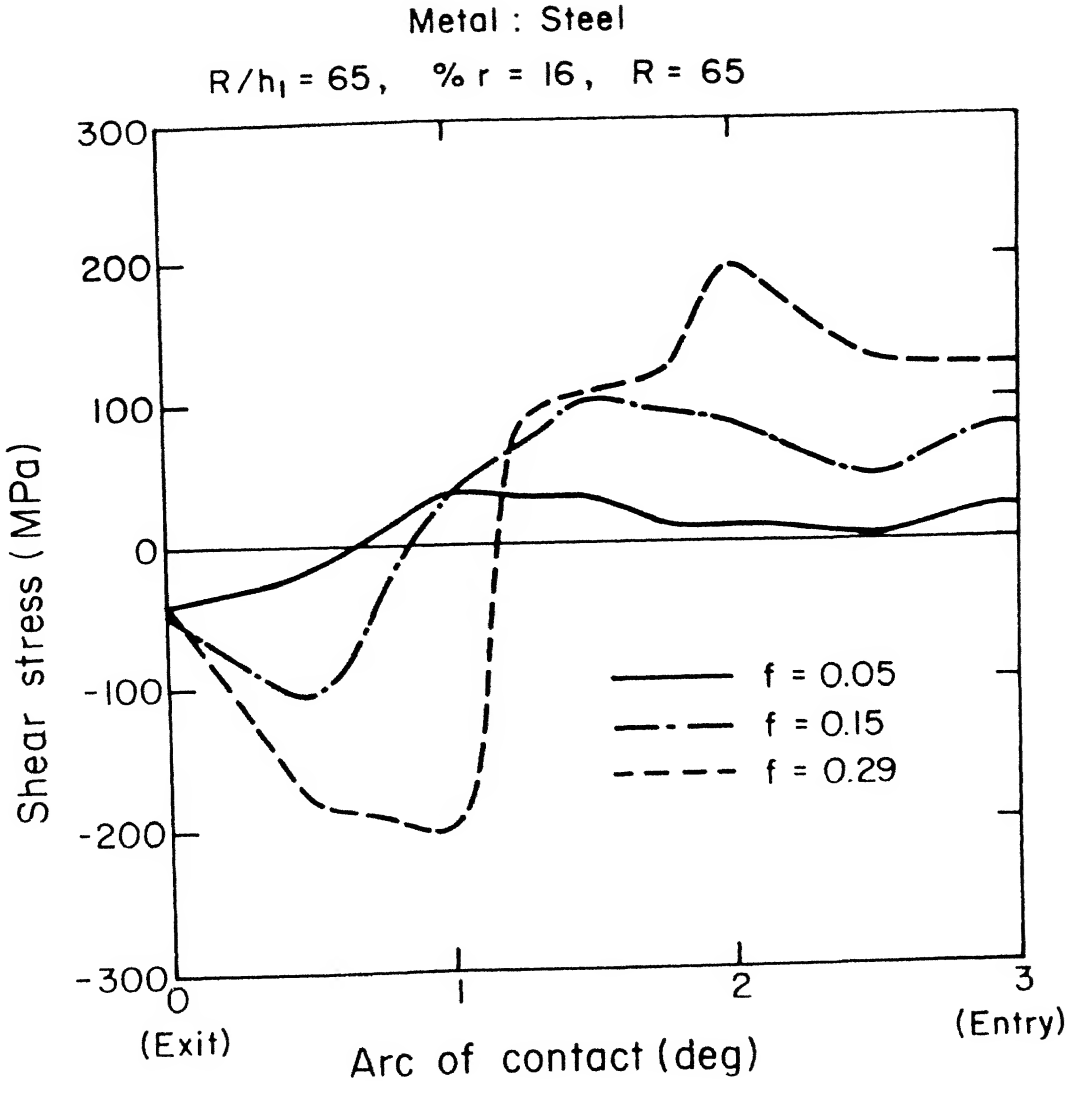

Fig.3.24 Distribution of shear stress at different coefficients of friction

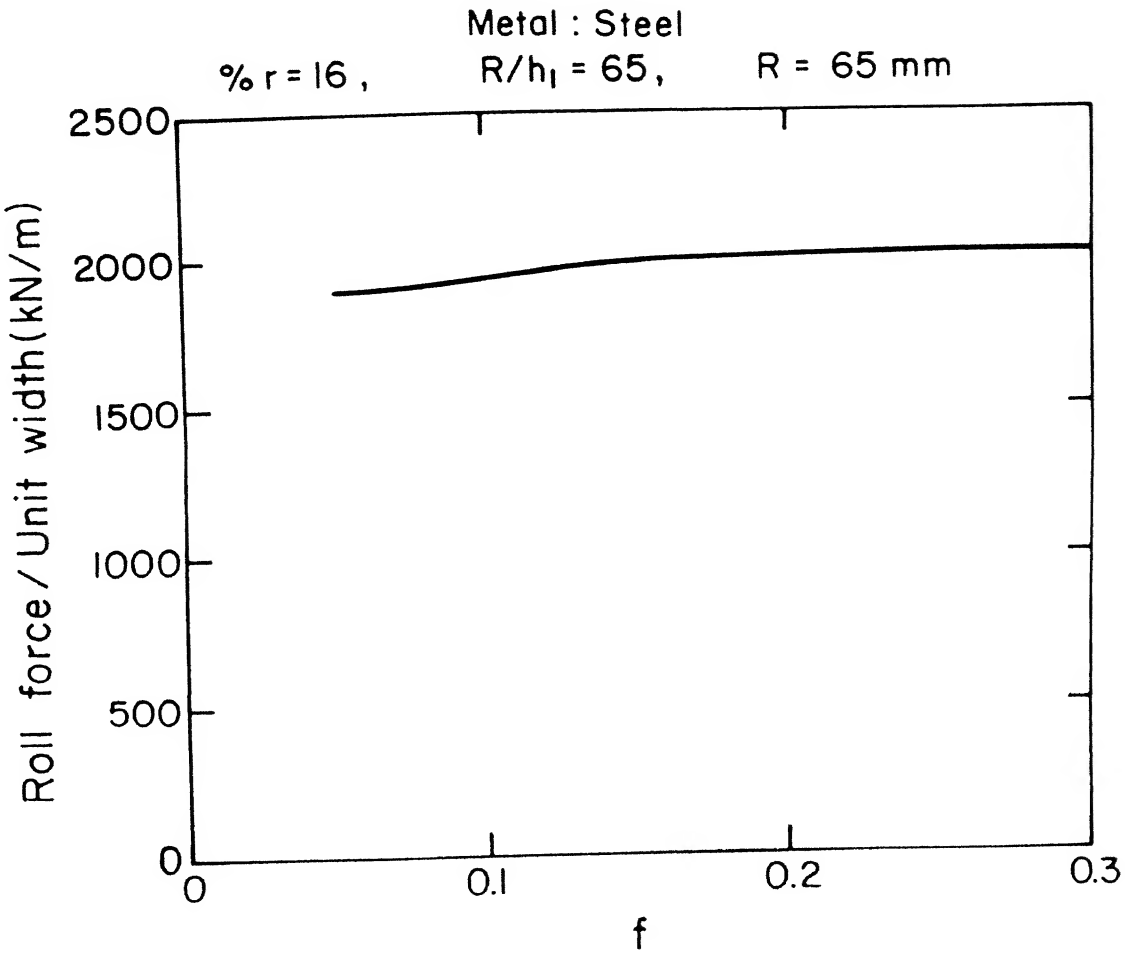

Fig.3.25 Variation of roll separating force with coefficient of friction

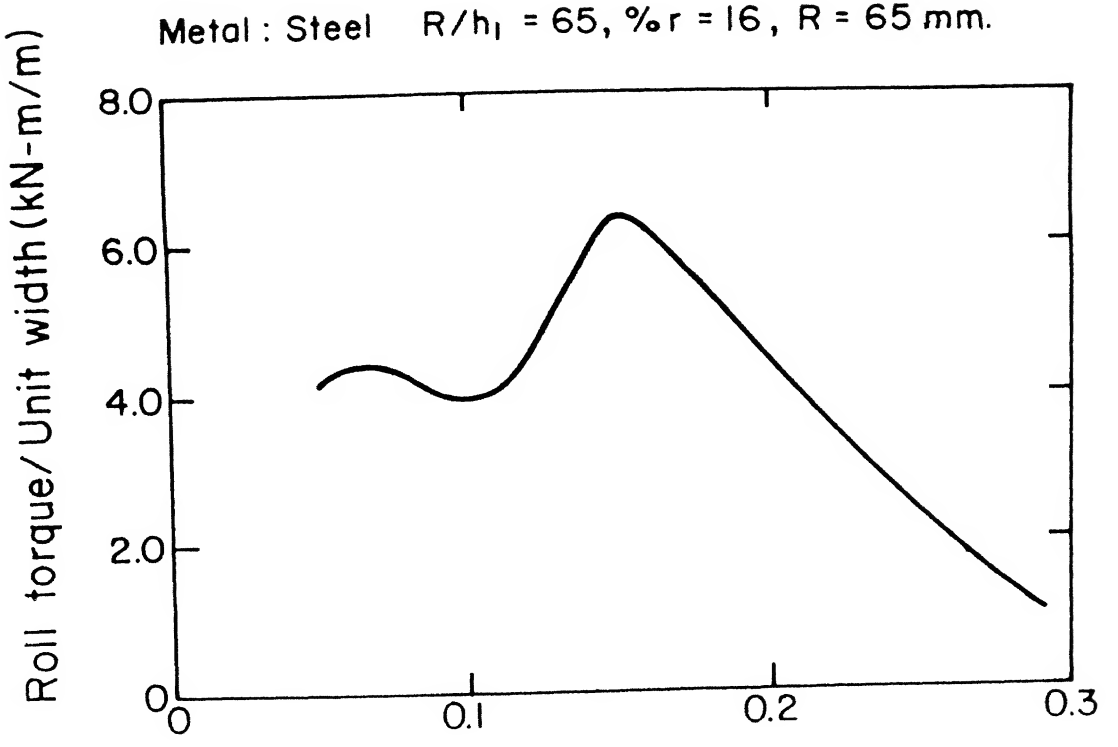

Fig.3.26 Variation of roll torque with coefficient of friction

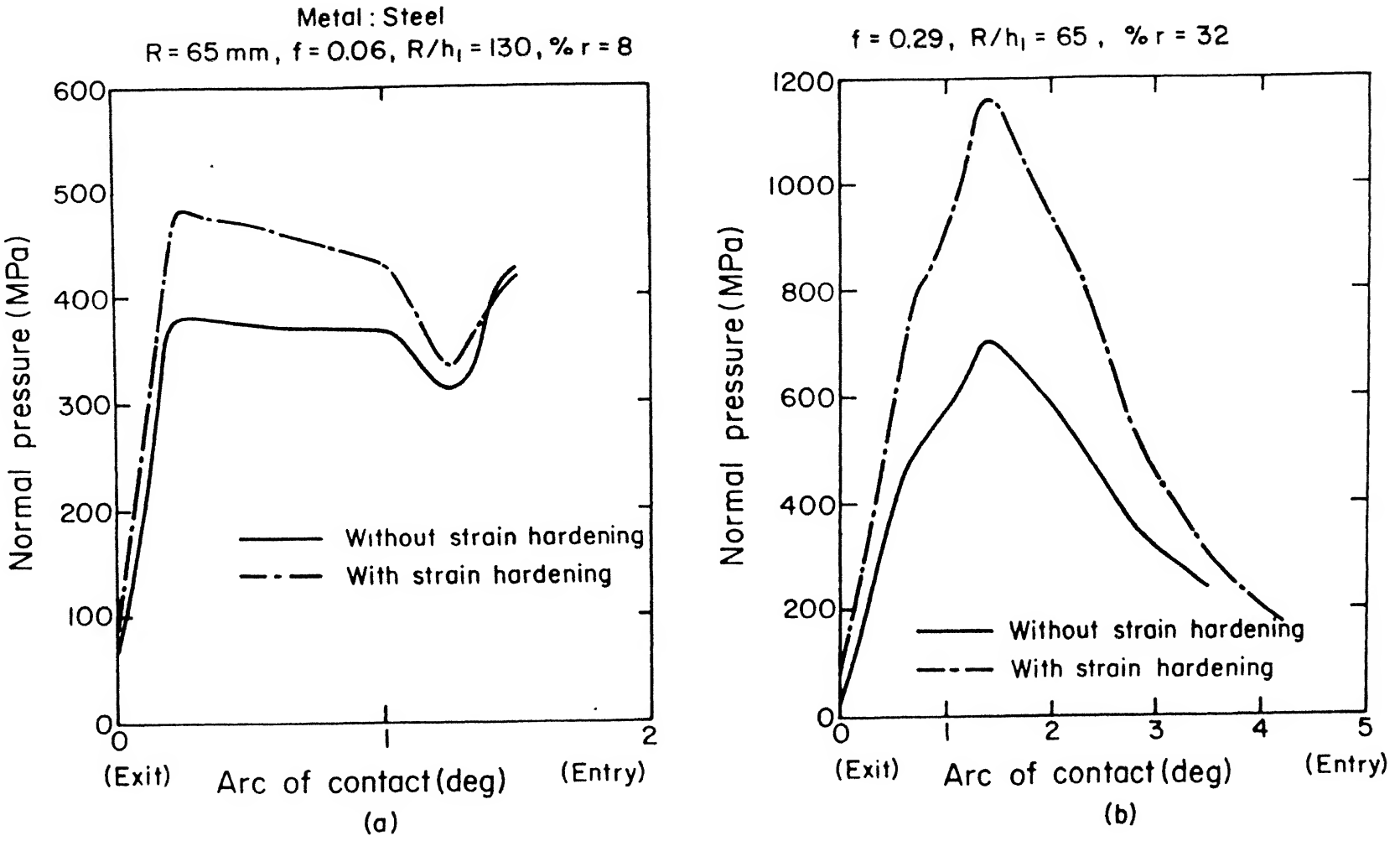

Fig3.27 Distribution of normal pressure with and without strain hardening (a) minimum and (b) maximum in the range.

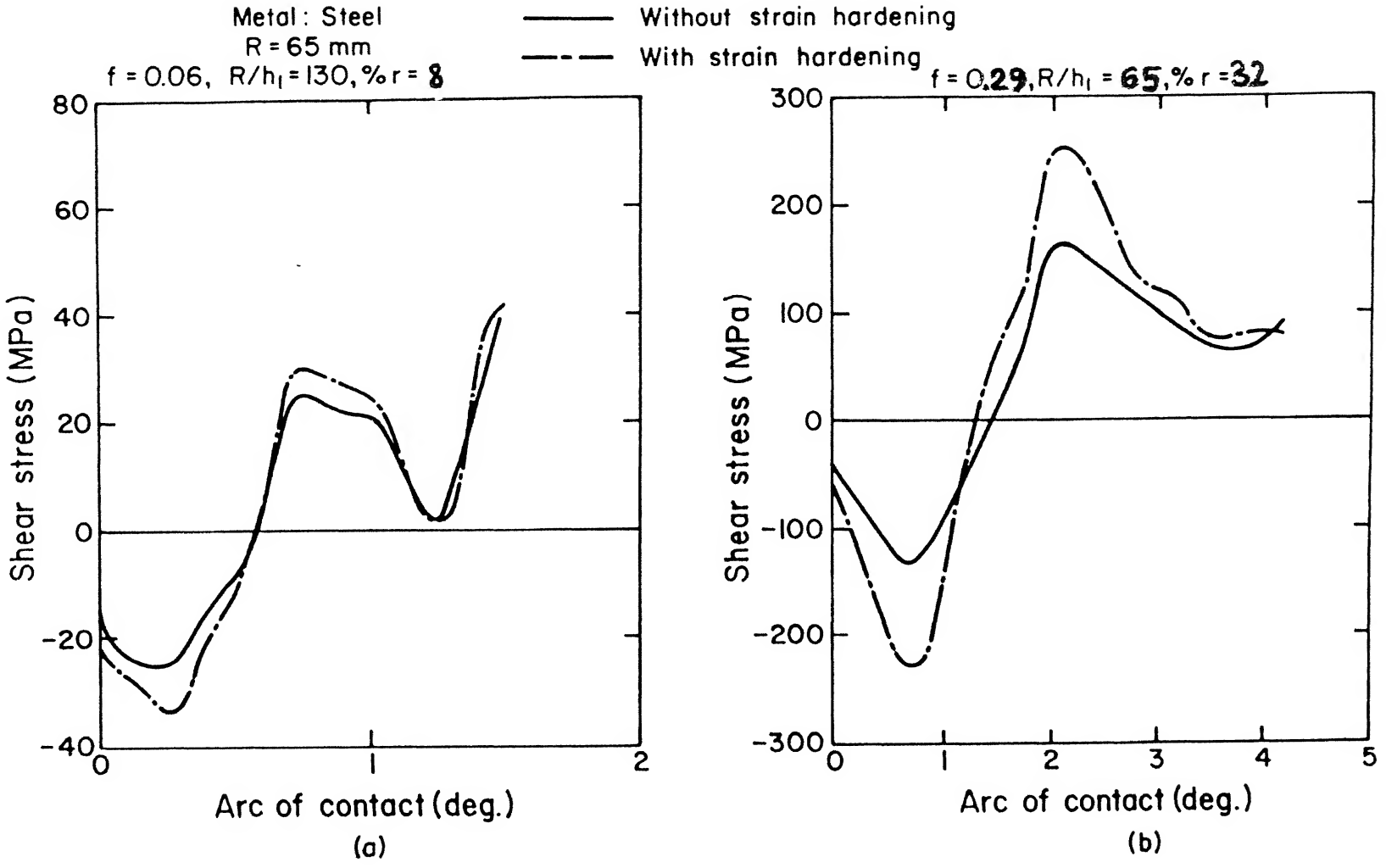

Fig.3.28 Distribution of shear stress with and without strain hardening (a) minimum and (b) maximum in the range

Table 1. Material Properties and Stress-Strain Relations

Material	Density (kg/m^3)	In the Relation, $\sigma_y=\sigma_o(1+K\bar{\varepsilon})^n$			Reference
		σ_o (MPa)	n	1/ K	
Aluminium	2800	50.3	0.260	0.050	Al-Salehi [25]
Steel	7870	358.0	0.300	0.044	Shida [26]
Steel	7870	324.0	0.295	0.052	Shida [26]
Copper	8600	70.3	0.490	0.022	Al-Salehi [25]

Table 2. The Percentage underestimation in the analysis without strain hardening for roll separating force, roll torque,peak magnitude of normal pressure and absolute peak magnitude of shear stress

Parameter	Set	Parameter Value		% Error (w.r.t. the value with strain hard.)
		without	with	
Roll Force (kN/m)	Set 1	596	707	15.70
	Set 2	2075	3111	33.45
Roll Torque (kN-m/m)	Set 1	1.06	1.15	07.82
	Set 2	11.13	16.35	31.93
$(t_n)_{max}$ (MPa)	Set 1	382	485	21.24
	Set 2	700	1160	39.66
$\lvert(t_s)\rvert_{max}$ (MPa)	Set 1	24	30	20.00
	Set 2	135	230	41.30

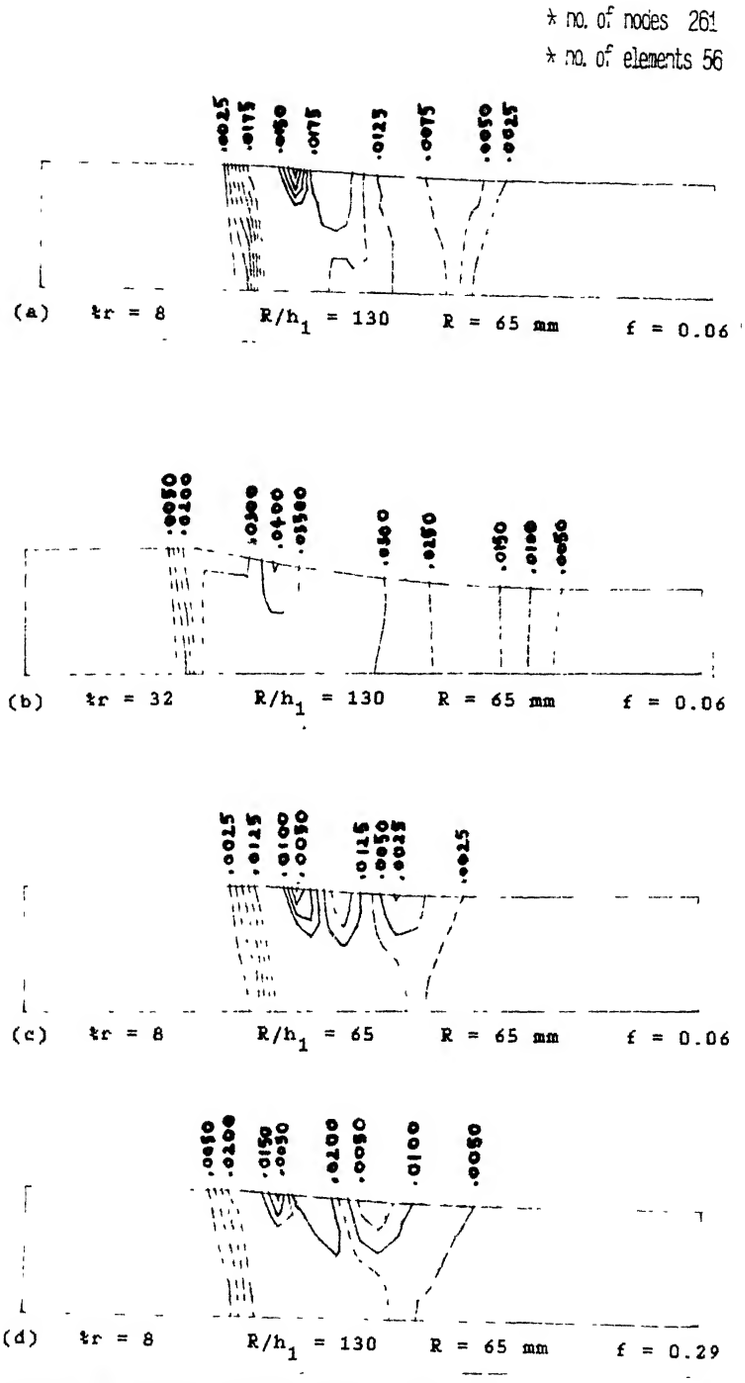

Fig. 3.29 Normal Strain-Rate Contours at Four Different Sets of Process Variables, (a), (b), (c) and (d).

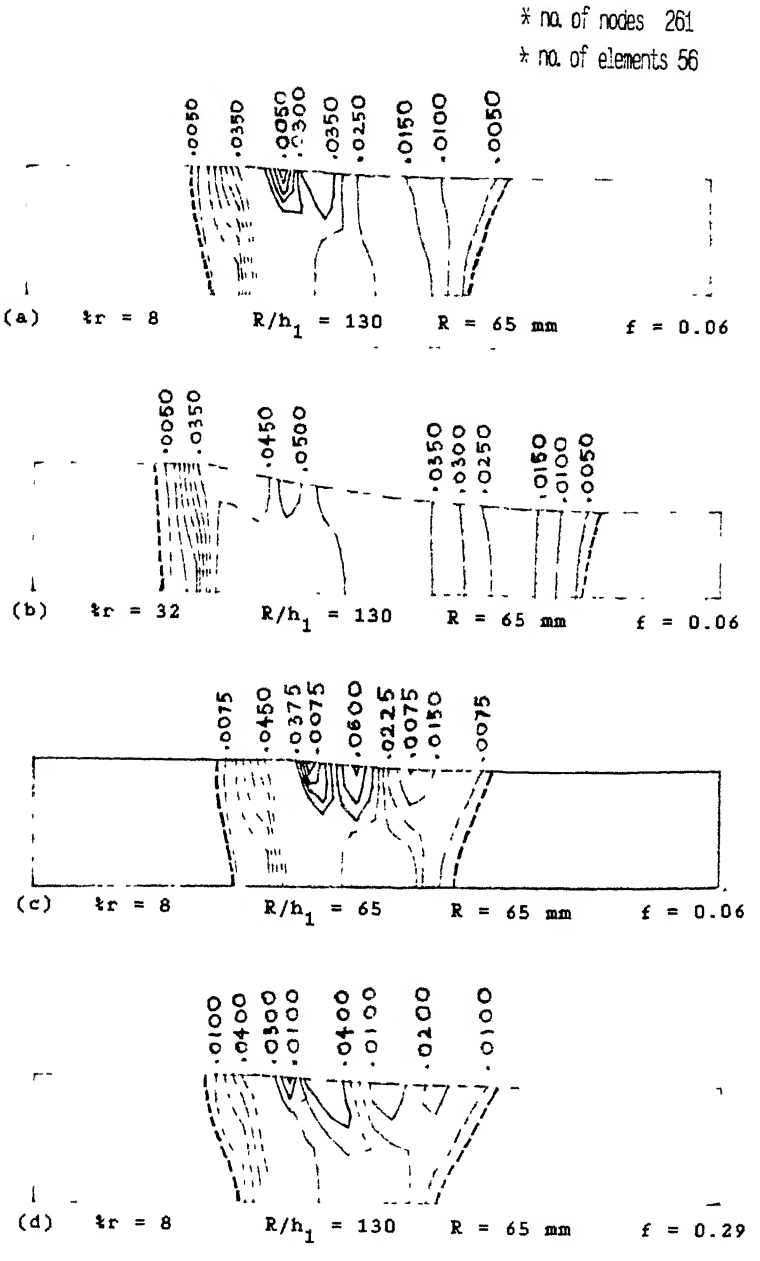

Fig. 3.30 Equivalent Strain-Rate Contours at Four Different Sets of Process Variables, (a),(b),(c) and (d)

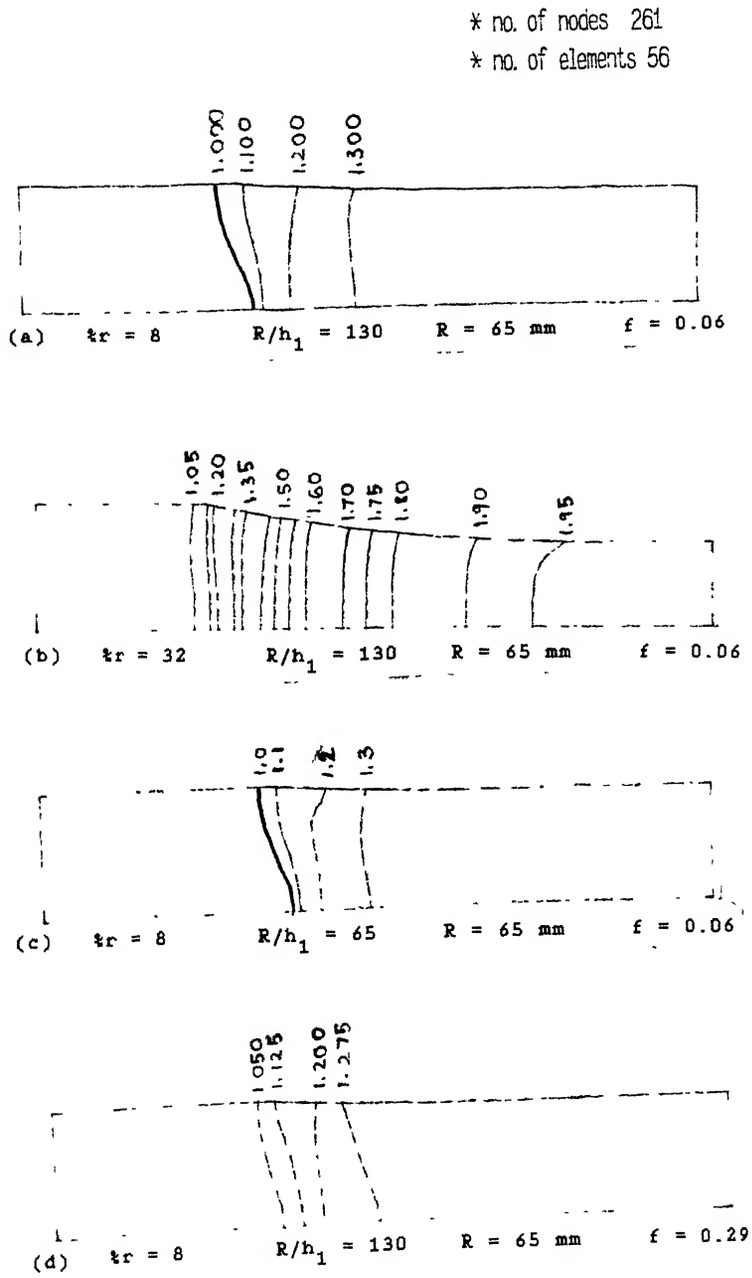

Fig. 3.31 Deviatoric Stress Invariant Contours at Four Different Sets of Process Variables, (a), (b), (c) and (d).

* no. of nodes 261

* no. of elements 56

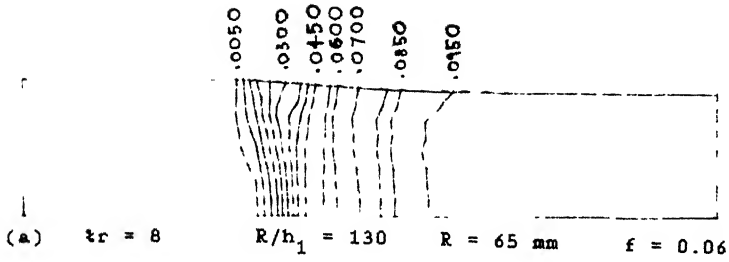

(a) t_r = 8 R/h_1 = 130 R = 65 mm f = 0.06

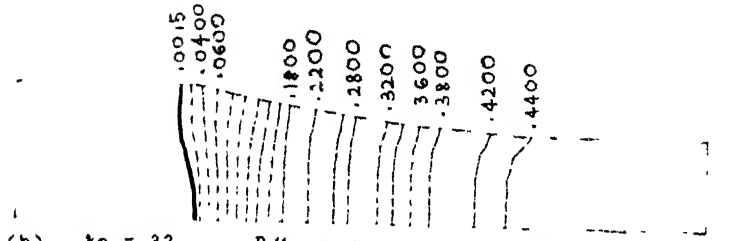

(b) t_r = 32 R/h_1 = 130 R = 65 mm f = 0.06

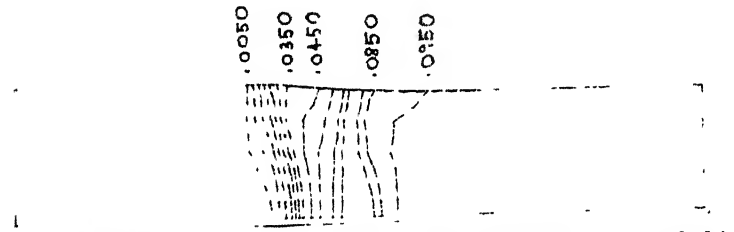

(c) t_r = 8 R/h_1 = 65 R = 65 mm f = 0.06

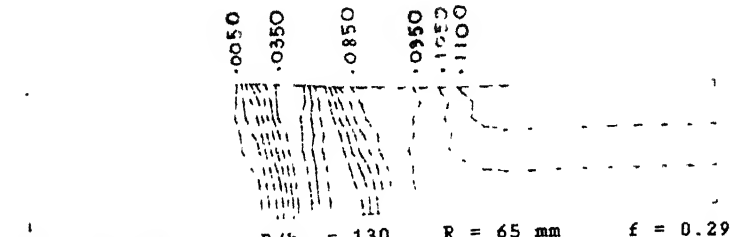

(d) t_r = 8 R/h_1 = 130 R = 65 mm f = 0.29

Fig. 3.32 Equivalent Strain Contours at Four Different Sets of Process Variables, (a), (b), (c) and (d).

REFERENCES

1. AVITZUR,B.," Metal Forming Processes and Analysis McGraw-Hill Company,New York,1970.
2. VON KARMAN,T.," On the theory of rolling ",Z.Angew Math. Mech.,Vol.5,1925,p.139.
3. OROWAN,E.," The Calculation of Roll Pressure in Hot and Cold Flat Rolling ",Proc.I.Mech.Engg.,Vol.150,1943,p.140.
4. BLAND,D.R., FORD,H.," The Calculation of Roll Force and Torque in Cold Strip Rolling with Tensions",Proc. I. Mech. E.,Vol.159,1948,p.144.
5. ALEXANDER,J.M.," On the Theory of Rolling ", Proc. R. Soc. of Lond.,Vol.A-326,1972,p.535.
6. LAHOTI,G.D.,SHAH,S.N.,ALTAN,T., " Computer-Aided Analysis of the Deformation and Temperatures in Strip Rolling", J. Engg. for Ind., Vol.100,1978,p.159.
7. ALEXANDER,J.M.," A Slip-Line Field For The Hot Rolling Process",Proc. I. Mech. E., Vol.169,1955,p.1021.
8. FIRBANK,T.C.,LANCASTAR,P.R., " A Suggested Slip-Line Field for Cold Rolling with Slipping Friction ", Int. J. Mech. Sci.,Vol.7,1965,p.847.
9. JOHNSON,W.,KUDO,H., " The Use of Upper-Bound Solutions for the Determination of Temperature Distribution in Fast Rolling and Axi-Symmetric Extrusion Process ",Int. J. Mech. Sci., Vol.1,1960,p.175.
10. ZIENKIEWICZ,O.C.,JAIN,P.C.,ONATE,E., " Flow of Solids During Forming and Extrusion : Some Aspects of Numerical Solutions ",Int. J. of Solids and Structures, Vol.14,1978,p.15.

11. DAWSON,P.R., " Viscoplastic Finite Element Analysis of Steady-State Forming Processes Including Strain History and Stress Flux Dependence ", Applications of Numerical Methods in Forming Processes ",AMD,Vol.28,1978,p.55.

12. LI,G.J.,KOBAYASHI,S.," Spread Analysis in Rolling by the Rigid-Plastic Finite Element Method ", NUMIFORM,1982,P.777.

13. Chen,C.C., and Kobayashi,S.," Rigid-Plastic Finite Element Analysis of Ring Compression, Applications of Numerical Methods to Forming Processes ",AMD,Vol.28,1978,p.163.

14. MORI,K.,OSAKADA,K.,ODA,T.," Simulation of Plane-Strain Rolling by Rigid-Plastic Finite Element Method ",Int. J. Mech. Sci.,vol.24,1982,p.519.

15. YHU-JEN HWU and LENARD,J.G.," A Finite Element Study of Flat Rolling ",ASME, J. Engg. Mat. and Tech., Vol.110,1988,p.22.

16. RICHELSON,A.B., " Viscoplastic Analysis of Plane-Strain Rolling Using Different Friction Models ",Int. J. Mech. Sci., Vol.33,No.9,1991,p.761.

17. PIETRZYK,M.," Rigid-Plastic Finite Element Simulation of Plane-Strain Rolling with Significantly Non-Uniform flow of Metal ", Proc. of NUMIFORM,1986,P.243.

18. MORI,K.,NAKADOI,K.,FUKUDA,M.," Coupled Analysis of Steady State Forming Process with Elastic Tools ",NUMIFORM,1986,P.237.

19. TOZAWA,Y.,ISHIKAWA,T.,IWATA,N., " Predicting the Profile of Rolled Strip ",NUMIFORM,1882,P.787.

20. LI,G.J.,KOBAYASHI,S.," Spread Analysis in Rolling by the Rigid-Plastic Finite Element Method ",NUMIFORM,1982,P.777.

21. BERTRAND,C.,DAVID,C.,CHENOT,J.L.,BUESSLER,P., " Stresses Calculation in Finite Element Analysis of 3-D Hot Shape Rolling ", NUMIFORM,1986,P.207.

22. LIU,C.,HARTLEY,P.,STURGERS,C.E.N.,ROWE,G.W., " Finite Element Modelling of Deformation and Spread in Slab Rolling ", Int. J. Mech. Sci.,Vol.29,1987,p.271.

23. LEE,Y.S.,DAWSON,P.R.,DEWHURST,T.B., " Bulge Predictions in Steady State Bar Rolling Processes ",Int. J. for Num. Meth. in Engg.,1990,p.1403.

24. MORI,K.,OSAKADA,K.," Finite Element Simulation of Three-Dimensional Deformation in Shape Rolling ", Int. J. Num. Meth. in Engg.,Vol.30,1990,p.1431.

25. AL-SALEHI,F.A.R.,FIRBANK,T.C.,LANCASTAR,.P.R.," An Experimental Determination of the Roll Pressure Determination in Cold Rolling ", Int. J. of Mech. Sci.,Vol.15,1973,p.693.

26. SHIDA,S.,AWAZUHARA,H.," Rolling Load and Torque in Cold Rolling ",J. Japan. Soc. Tech. Plast., Vol.14,1973,p.267.

27. BERCOVIER,U.,ENGLEMAN,M., " A Finite Element for the Numerical Solution of Viscous Incompressible Flows",J. of Computational Physics, Vol.30,1979,p.181.

28. TSELIKOV,A.I., ZYUZIN, V.I., " Modern Development of Rolling Mills " , MIR Publishers, Moscow, 1972.

BRIEF BIBLIOGRAPHY

1. HILL,R.," THE MATHEMATICAL THEORY OF PLASTICITY ", Oxford Press,1950.
2. CRANDALL,S.H.,DAHL,N.C.,(editors)," An Introduction to the Mechanics of Solids " ,McGraw-Hill Book Company,New York,1959.
3. JOHNSON,W., MELLOR, P.B., " Plasticity for Mechanical Engineers " , Van Nostrand, Princeton, New Jersey, 1962.
4. THOMSEN, E.G., YANG, C.T., KOBAYASHI, S., " Mechanics of Plastic Deformation in Metal Processing " , The Macmillan Company, New York, 1965.
5. GOPINATHAN, V., " Plasticity Theory and its Applications in Metal Forming " , Wiley Eastern Publishers, New Delhi, 1982.
6. JAVORONKOV,V.A., CHATURVEDI, R.C., " Rolling of Metals " , Yantrik, Bombay, 1981.
7. THOMSEN,E.G.,BERMAN,M., " Steady State Analysis of Elasto Viscoplastic Flow During Rolling ", NUMIFORM,1982,P.29.
8. SASTRY, S.S., " Introductory Methods to Numerical Methods " , Prentice- Hall of India, New Delhi, 1987.
9. KOBAYASHI,S.," Metal Forming and the Finite Element Method ", Oxford Press, 1990.
10. Cook, R.D., " Concepts and Applications of Finite Element Analysis " , John Wiley & Sons, New York, 1981.